TECHNISCHE UNIVERSITÄT WIEN
Vienna | Austria

Diploma Thesis

Aging of reinforced thermoplastic pipes under extreme environmental conditions

carried out for the purpose of obtaining the degree of Dipl.-Ing. submitted at the Institute of Materials Science and Technology at Vienna University of Technology

under the supervision of

Senior Scientist Dipl.-Ing. Dr.techn. Thomas Koch

and

Ao.Univ.Prof. Dipl.-Ing. Dr.mont. Vasiliki-Maria Archodoulaki

by

Matthias Otto Kapfhammer

[redacted]

Affidavit

I declare in lieu of oath, that I wrote this thesis and performed the associated research myself, using only literature cited in this volume. If text passages from sources are used literally, they are marked as such.
I confirm that this work is original and has not been submitted elsewhere for any examination, nor it is currently under consideration for a thesis elsewhere.

Vienna May 17, 2020

Signature student

Danksagung

An dieser Stelle möchte ich mich bei allen bendanken, die mich in den Jahren des Studiums unterstützt haben und mir dieses überhaupt erst ermöglicht haben. Meinen Betreuern Senior Scientist Dipl.-Ing. Dr.techn. Thomas Koch, Ao.Univ.Prof. Dipl.-Ing. Dr.mont. Vasiliki-Maria Archodoulaki und Dipl.-Ing. Dr.techn. Christoph Schoberleitner gilt ein besonderer Dank, da sie mir jederzeit für Fragen und Hilfestellungen zur Seite standen.

Auch meiner Familie und besonders meinen Eltern möche ich einen großen Dank aussprechen. Sie haben mir mein Studium in dieser Form erst ermöglicht.

Dass meine Studieunzeit zu einer Zeit wurde, die ich keinesfalls missen möchte, haben meine Studienkollegen besonders beigetragen. Diese Zeit wird mir immer in Erinnerung bleiben. Nennen möchte ich hier besonders Otmar, Michi, Christian und Tobi. Ich danke euch für die zahlreichen Stunden in denen wir unser Studentendasein gefristet haben.

Auch Luzia, die mich in dieser letzten Phase meines Studiums immer unterstützt hat, gilt mein besonderer Dank.

Abstract

The aim of the thesis was to make a statement about the usability of reinforced thermoplastic pipes (RTP) which are used for the oil industry after natural ageing. The pipes were never used but stored for almost ten years under extreme environmental conditions in the Middle East. This made it necessary to investigate the pipes by various methods like thermal analysis, mechanical analysis and optical analysis to determine the material properties and to find out whether ageing has taken place and if the pipes can be used without safety concerns.

The first important information was the composition of the materials of the pipes. The liner and the outer jacket were made of polyamide 6 (PA6) and the textile was made of aramid (PPTA). The visual inspection shows external damage. The jackets of the pipes were coated with microcracks and the exposed areas of the liners were fissured. Furthermore, it was discovered, that the liner is built up of three layers about the cross section, which can be recognized by the different colours of the single layers. These layers were expected to come from different crystalline phases.

No reference material was available, so the obviously intact material of the pipes was compared with the brittle material at the end of the pipes. The differential scanning calorimetry (DSC) and the Fourier-transform infrared spectroscopy (FTIR) did not show distinctive ageing effects. The thermogravimetric analysis showed that the PA6 of the liner must be filled with a softener. Tensile test and notched Charpy impact test confirmed this thesis by the low Young‘s modulus and high impact strength. The FTIR also confirmed that the various layers of the liner were not attributable to crystalline phases. In summary the pipes show reasonably good conditions for their envisaged usage.

Zusammenfassung

Ziel der Diplomarbeit war es, eine Aussage über die Verwendbarkeit von verstärkten thermoplastischen Rohren (RTP) für die Ölindustrie, die einer natürlichen Alterung unterlegen sind, zu treffen. Die Rohre wurden nie verwendet, jedoch für fast zehn Jahre unter extremen Umweltbedingungen im Mittleren Osten gelagert. Daher war es nötig, die Rohre mittels verschiedener Methoden wie thermischer, mechanischer und optischer Analyse zu untersuchen, um deren Materialeigenschaften herauszufinden und zu bestimmen, ob Alterung stattgefunden hat. Daraus war eine Aussage über die bedenkenlose Verwendbarkeit der Rohre zu treffen.
Die erste wichtige Information, die aus den Ergebnissen resultierte, war die Zusammensetzung der einzelnen Rohrmaterialien. Die innere Auskleidung und der Mantel wurden aus Polyamid 6 (PA6), die Verstärkung aus Aramid (PPTA) gefertigt. Die optische Begutachtung zeigte äußere Schäden. Der Mantel der Rohre war mit Mikrorissen überzogen und auch die freiliegenden Bereiche der inneren Auskleidung waren rissig. Weiters zeigte sich, dass in der Auskleidung drei verschiedene Schichten auftreten, die sich durch verschiedene Farben des Materials äußerten. Es wurde vermutet, dass es sich um verschiedene kristalline Phasen handle. Da kein Referenzmaterial verfügbar war, wurde das vermeintlich nicht gealterte Material mit jenem der mit Rissen durchzogenen Enden der Rohre verglichen. Die dynamische Differenzkalorimetrie (DSC) und die Fourier- Transformations- Infrarotspektroskopie (FTIR) zeigten keine markanten Alterungseffekte. Die thermogravimetrische Analyse (TGA) deutete darauf hin, dass das PA6 der inneren Einlage mit einem Weichmacher versetzt ist. Der Zugversuch und der Kerbschlagbiegeversuch bekräftigten auf Grund des niedrigen E-Moduls und der geringen Zugfestigkeit diese Vermutung. Die FTIR zeigte auch, dass die verschiedenen Farben in der Einlage nicht durch unterschiedliche kristalline Phasen sondern durch andere, nicht näher bestimmte Effekte, entstanden sind. Alles in allem zeigen die Rohre gute Eigenschaften für einen geplanten Einsatz.

Contents

1 Introduction **1**

1.1 Objective . . . 1

1.2 Samples . . . 2

1.2.1 General information . . . 2

1.2.2 Liner . . . 4

1.2.3 Reinforcement . . . 5

1.2.4 Jacket . . . 7

1.3 Polyamide . . . 9

1.3.1 Polymeric Structure . . . 10

1.3.2 Chemical Composition . . . 10

1.3.3 Microstructure . . . 11

1.4 Properties . . . 12

2 Methods **14**

2.1 Thermal Analysis . . . 14

2.1.1 DSC . . . 14

2.1.2 TGA . . . 16

2.2 Mechanical Analysis . . . 18

2.2.1 Tensile Test PA6 . . . 18

2.2.2 Tensile Test Aramid . . . 21

2.2.3 Charpy Notched Impact Test . . . 21

2.3 Optical Analysis . . . 25

2.3.1 FTIR . . . 25

2.3.2 EDX . . . 26

2.3.3 Dye Penetrant Test . . . 27

3 Results 28
3.1 DSC . . . 31
3.1.1 Jacket . . . 36
3.2 FTIR . . . 37
3.3 TGA . . . 46
3.3.1 TGA Aramid . . . 51
3.4 Tensile Test . . . 54
3.4.1 Tensile Test Aramid . . . 56
3.5 Charpy Notched Impact Test . . . 58
3.6 EDX . . . 59

4 Conclusion 60

Bibliography i

1 Introduction

1.1 Objective

Polymeric materials are used more and more for pipe systems in the oil industry as a replacement for conventional steel pipes. Advantages are better corrosion resistance, flexibility, low density by high-pressure capability and cost-effectiveness. The underlying task of this diploma thesis is the investigation of unused reinforced thermoplastic pipes (RTP) for the petrol industry. These multilayered pipes were exposed to outdoor weathering conditions of the Middle East for approximately ten years. The coils on which 700 metres of pipes were furled, were covered only with a tarpaulin. The climate in this area is very hot with high humidity and little rainfall. Due to the fact that the environmental conditions under which the pipes were stored for such a long time are not known exactly, it is hard to predict the condition of the tubes. A major problem is that the materials which the RTP are made of, are not known exactly and material datasheets are not available for every single layer. This means that first the material of every layer has to be determined before it can be compared with material characteristics from the literature. Initial speculations suggesting that it was polyamide, the exact type still had to be determined.

The pipes were tested with thermal, mechanical and optical methods to find out whether they can still be used without safety concerns. Loads like high temperature, high humidity and UV radiation, which have dominated the environmental history of this piping material, are important factors which accelerate ageing and degradation mechanisms.

1.2 Samples

1.2.1 General information

The materials to be tested are high-pressure pipes for the oil industry. Four ends of the coiled-up pipes were available to investigate and were numbered from 1-4. The pipe sections with a length of approximately 130cm are shown in figure 1.1 - 1.4.

Figure 1.1: Pipe 1

Figure 1.2: Pipe 2

Figure 1.3: Pipe 3

Figure 1.4: Pipe 4

According to the imprint which is located on the pipes, they have an outer diameter of 4,55in (≈ 12cm) and can stand pressure up to 750psi (≈ 52bar) under a temperature of 150°F (≈ 66°C). The imprint can be seen in figure 1.5.

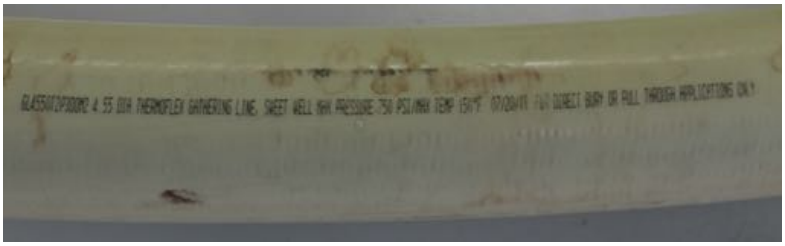

Figure 1.5: Imprint on pipe 3

The exact material of liner and jacket is unknown, only for the reinforcement a datasheet is available. A pre-test with DSC and FTIR showed that liner and jacket are made of polyamide 6 (PA6). To better evaluate and compare the material parameters obtained in the remaining analyses, the pre-tests were carried out before all other analyses. The exact evaluation of the material composition is discussed in chapter 3 Results.

The general construction of the pipes consists of three layers:

- Liner
- Reinforcement
- Jacket

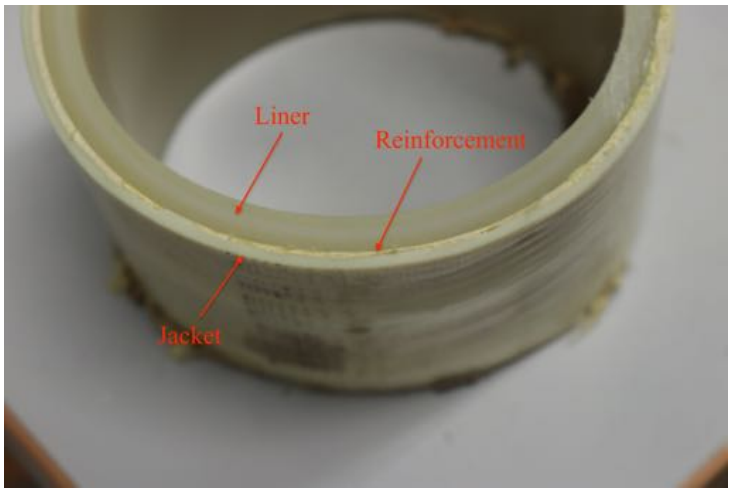

Figure 1.6: Cross section

1.2.2 Liner

The liner has the function of taking the main load. It consists of ≈ 6,6mm thick, extruded PA. It can be observed on each of the four pipes, that in a small area on the very end of the pipe section where the liner is not covered with reinforcement and jacket, the liner is brittle and covered with cracks. Thus it can be concluded, that the liner is aged in this area. This can be seen in figure 1.7 - 1.10. The sample 1R, which acted as a representative sample for the aged area of all four pipes, was taken from the uncovered area of pipe 1, shown in figure 1.7.

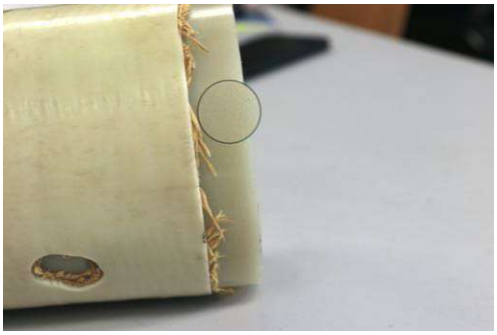

Figure 1.7: End of pipe 1

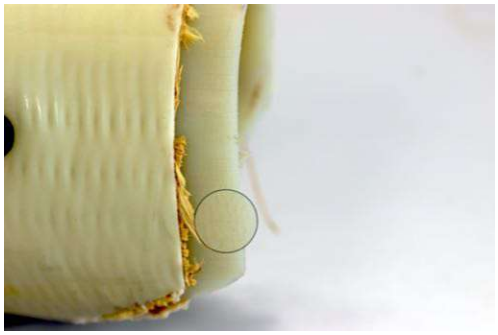

Figure 1.8: End of pipe 2

Figure 1.9: End of pipe 3

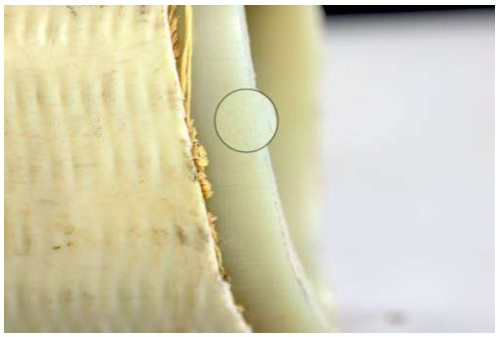

Figure 1.10: End of pipe 4

1.2.3 Reinforcement

The reinforcement consists of two components, both made of PPTA yarn. The first one is the longitudinal yarn which is only put lengthwise on the liner but not woven. It can be seen in figure 1.14. It does not enclose the tube over the circumference as shown in figure 1.12. The second component is the braided yarn. As it can be seen in figure 1.13, three parallel yarns are cross-woven for the fabric. It is woven over the liner with the applied longitudinal yarn. The longitudinal and braided yarn are not interwoven. It can be observed, that the inside of the reinforcement has another colour than the outside.

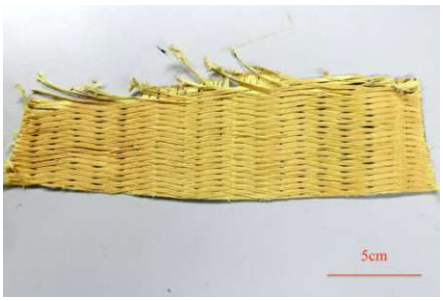

Figure 1.11: Reinforcement outside

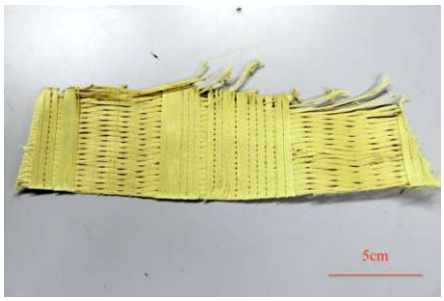

Figure 1.12: Reinforcement inside

Figure 1.13: Reinforcement braided

Figure 1.14: Reinforcement longitudinal

According to the research note [1], the reinforcement is made of Twaron 1008 yarn - 1680 dtex Z90. Figure 1.15 gives a short overview of the properties of the single types of Twaron 1008 yarns. The yarn used for the RTP has a breaking

strength of 360 N with an elongation at break of 3,45%, measured at a twist level of 90 turns per meter.
The twist level gives the spiral turns per length unit around the longitudinal axis, which are applied to the yarn. [2]

Twaron 1008 (dtex)		1100 F1000	1680 F1000	2520 F1000	3360 F2000
Linear density	dtex	1135	1735	2600	3500
Breaking strength	N	242	360	530	705
Elongation at break	%	3.35	3.45	3.8	3.6
Force at specified elongation 1%	N	62	88	117	170
Loop breaking strength	N	211	310	431	643
Chord modulus	GPa	80	72	67	72
Measured at twist level	tpm	120	90	75	60

Figure 1.15: Properties of various Twaron type 1008 yarn [3]

In figure 1.16 the dependence of the breaking strength to the twist level is shown. One can see that for 1680 dtex the breaking strength changes about 100N between 0tpm and 90tpm.

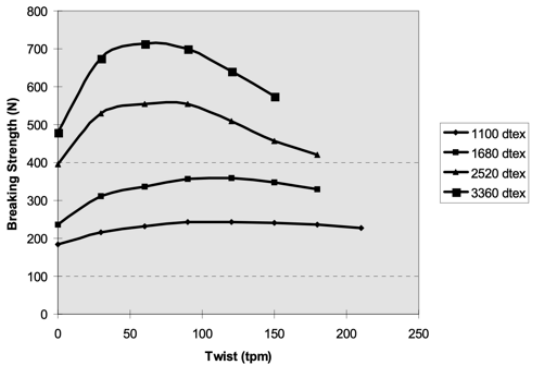

Figure 1.16: Breaking strength of Twaron type 1008 at various twist levels [3]

When interwoven, the yarn should have a twist level of 90tpm according to 1.15. If the twist level can be maintained when detaching the single yarn fibres from the textile for measuring can not be said for sure. A twist tester would be needed to specify the level of twist.

1.2.4 Jacket

The outer layer which has the main function to protect the pipe from mechanical damage is also made of PA6. All of the four jackets are having cracks on their surface as it is shown in figure 1.17 - 1.20. They do not occur exactly in the same extent on every pipe but it can be observed, that the side which was on the inside of the coil is not that affected as the outside. This can be well observed at the jacket of pipe 3.

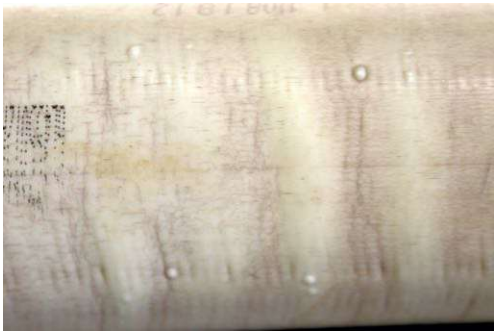

Figure 1.17: Jacket pipe 1

Figure 1.18: Jacket pipe 2

Figure 1.19: Jacket pipe 3

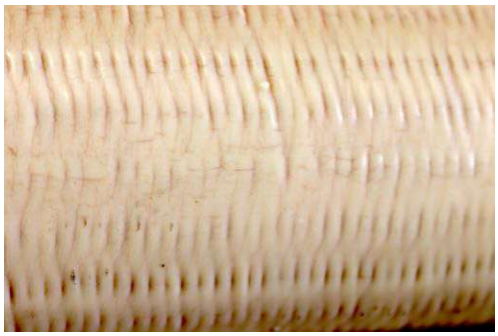

Figure 1.20: Jacket pipe 4

The fact, that it is extruded directly onto the textile makes it hard to determine the exact thickness because the PA has adapted to the fibres as it can be seen in figure 1.21.

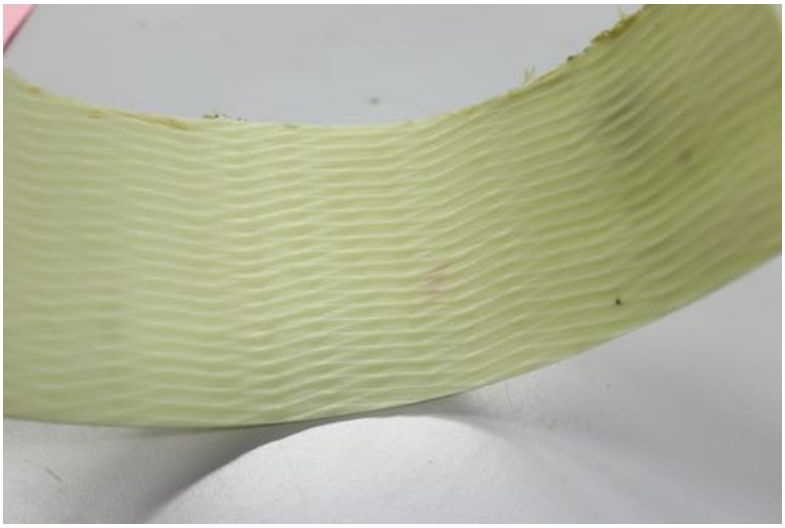

Figure 1.21: Inside of the jacket

1.3 Polyamide

Since the beginning of time, the raw materials which are available for humans are playing a decisive role in their lifes. Even the periods of time like stone age, bronze age and so on are named after these materials. Already in the medieval times, people substituted natural horn with products made of milk protein (casein). After this chemical modified natural materials, Leo Hendrik Baekeland developed 1872 the first fully synthetic plastic called Bakelit. In the first half of the 20th century, plastic started its success story. The worldwide production of plastics shows since the early 1900s an exponential growth so that Karl Mienes founded the term "Kunststoffzeitalter" (Plasticaeum) for the latest chapter of human history. [4]
All polyamides (PA) have in common that the amide (-CONH-) like in figure 1.22 occurs repeatedly in the polymer. This Materials can be fibres, crystalline or amorphous plastics, adhesives and rubbers. The first polyamide was polyamide 66 (PA66), it was synthesized 1935 by W. H. Carothers via condensation polymerisation. The DuPont Company started to commercialize the production of PA in December 1939 and they sold the product under the name Nylon, which is colloquial for almost every polyamide nowadays. [5]

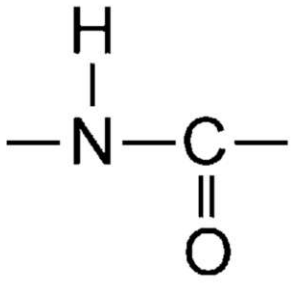

Figure 1.22: -CONH- group[6]

1.3.1 Polymeric Structure

The Polyamides can be classified in three groups by means of the polymeric structure:

- aliphatic polyamide
- semi-aromatic polyamides
- aromatic polyamides

Only aliphatic polyamides have linear or branched aliphatic hydrocarbon units. The other two groups contain monomers with conjugated systems.

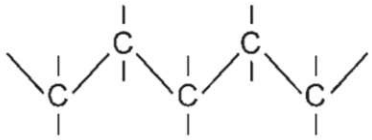

Figure 1.23: Aliphatic molecule [6]

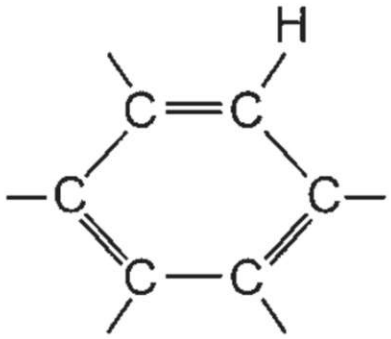

Figure 1.24: Aromatic molecule [6]

1.3.2 Chemical Composition

The structural formula indicates the basic module of the polyamide. Either it is one monomer which contains both, the amine and the carboxyl group (AB polymers) or the polyamide is built of two basic modules in which the amine and the carboxylic acid groups are grouped (AA/BB polymers). A typical example of an AB polymer is PA6. The 6 in the structural formula gives the number of carbon atoms in the monomer which is ϵ - caprolactam in this case.

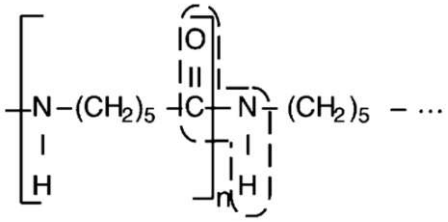

Figure 1.25: PA6 with -CONH- group [6]

PA66 is a representative of AA/BB polymers. The first number stands for the number of carbon atoms in the diamine and the second number for the number of carbon atoms in the dicarboxylic acid. The two basic monomers at PA66 are hexamethylene diamine and adipic acid.
A third group are the copolyamides. They are synthesized by more polyamide forming monomers. PA66/6 for example is formed by the homopolymers PA66, whose monomers are hexamethylene diamine and adipic acid and PA6 whose monomer is caprolactam. [7]

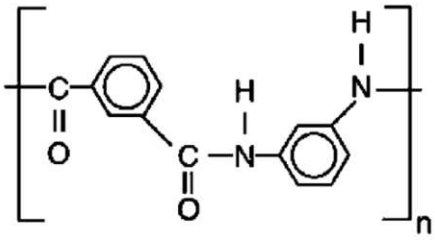

Figure 1.26: PPTA [6]

1.3.3 Microstructure

The microstructure allows another division, in semi-crystalline polyamides and amorphous polyamides. The semi-crystalline polyamide contains amorphous and crystalline domains. Amorphous polyamides contain only amorphous domains without any long-range order between the repeated units. The cooling condition is an important factor for crystallinity. A high cooling rate produces small crystalline regions with a low degree of crystallinity whereas a slow cooling process results in larger crystalline areas with a higher degree in crystallinity. [7]

1.4 Properties

The amide group (-CONH-) and the hydrocarbon residues are strongly determining the properties of polyamides. They are forming hydrogen bridge bonds in the amorphous domains which leads to the crystalline structures. The good mechanical properties of PA like high Young's modulus, materials toughness or the heat resistance can be reduced on this hydrogen bridge bonds. In the amorphous regions, the polar amide functionalities can interact with smaller polar molecules. The most important representative is water. Conditioning, how the absorption of water in polyamides is called, essentially affects the properties. [7]

The more often the amide group occurs in the chain connection, the higher are the intermolecular forces and the more water can be picked up by the PA which again gives the PA high impact strength, high abrasive resistance, and good gliding properties. This illustrates, that one problem of PA is, that the mechanical properties are linked with the conditioning. [8]

Also, the number of methylene (-CH_2-) groups has a substantial influence on the characteristics of PA. With an increasing number, the distance of the amide functionalities is also increasing what leads to a decrease of the intermolecular forces. As an example, PA12 is softer than PA6 and has a lower melting temperature T_m. [7]

Figure 1.27 shows the molecular structure of PA6 and PA66. At PA66 the amide groups face each other directly what means that every functional group can built a hydrogen bridge bond without deformation of the molecules. At PA6, only every second amide group can built a hydrogen bridge bond what leads to a lower melting temperature of PA6. [9]

Symmetric hydrocarbon residuals resulting in a higher degree of crystallinity because the amide groups are in a position, that every functional group can create a hydrogen bridge bond without a deforming of the molecules. [7] [9]

This can be seen in figure 1.27

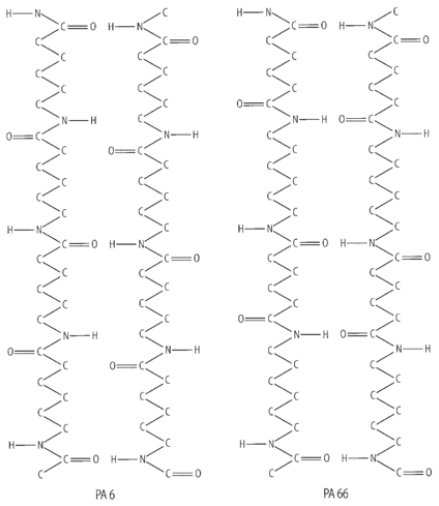

Figure 1.27: Molecular structure of PA6 and PA66 [9]

Aliphatic polyamide like PA6 have a very low glass transition temperature T_g, which is in the range of room temperature and therefore not that easy to be detected. The fact, that PA is semi-crystalline makes them applicable near to their melting temperature. Polyamides are resistant to various substances like solvents, oils, fats, fuels, weak alkalis, ketones and boiling water. This means that they can be sterilized. Whereas sulfuric and formic acids are good solvents. [7]
Long-chain synthetic polyamides, which have more than 85% of the amide groups directly bonded with aromatic rings, called per definition aramids. Fibres made of poly(p-phenylene terephthalamide) (PPTA) are those with the highest specific strength of all commercial fibres. Due to the fact, that the melting temperature of polyphenylene phthalamide is higher than its degradation temperature, it is not possible to melt spin the fibres. PPTA is dissolved in concentrated sulfuric acid and spun into highly crystalline fibres with strong molecular orientation what leads to their very high strength, high impact resistance and high elongation at break. In combination with the low density of only 1,45 g/cm^3, PPTA develops its high weight-specific strength. The golden/yellow fibres are very heat resistant. The glass transition temperature of the fibres is about 300°C and at temperatures above 400°C they begin to char. As all PA, PPTA is hygroscopic. It takes up water up to 7%. [7]

2 Methods

2.1 Thermal Analysis

2.1.1 DSC

Identification of polymers is one of the main applications for DSC measuring. This method can identify transition temperatures like glass temperature T_g, melting temperature T_m or crystallisation temperature T_c. In figure 2.1 a DSC measuring cell using the heat-flow principle is shown. The measuring cell can be seen as a small oven with two bean-sized aluminium pans. One pan is filled with the sample, the other with a reference material which is usually air. The pans are heated simultaneously following a given temperature program. The heat flow of the sample plan is continuously compared to the heat flow of the reference pan. If the heat flow changes during phase transformations in the sample whereas the heat flow in the reference pan stays stable as before, the difference can be seen as a peak in the plot. The peaks can either show an endothermic or exothermic reaction. If the reaction is endothermic, the sample absorbs heat as it does in a melting process, the heat flow in the sample pan is higher than in the reference pan. If the reaction is exothermic, the heat flow in the sample pan is lower and the sample emits heat. This is what happens at a crystallisation process. In table 2.1 different causes are dedicated to either exothermic or endothermic reactions. [10]

"Differential Scanning Calorimetry (DSC) means the measurement of the change of the differential in the heat flow rate to the sample and to a reference sample while they are subjected to a controlled temperature program." [11]

Table 2.1: Physical and chemical causes for DSC peaks [10]

Physical causes			Chemical causes		
	Endothermic	Exothermic		Endothermic	Exothermic
Melting	x		Chemisorption		x
Crystallization		x	Desolvation	x	
Evaporation	x		Dehydration	x	
Sublimation	x		Degradation	x	
Adsorption		x	Oxidative degradation		x
Absorption	x		Redox reaction	x	x
Desorption	x		Solid phase reaction	x	x
Curie temperature transitions	x		Combustion		x
Liquid-crystal transitions	x		Polymerisation		x
Glass transition	No peak, only shift		Curing, crosslinking		x

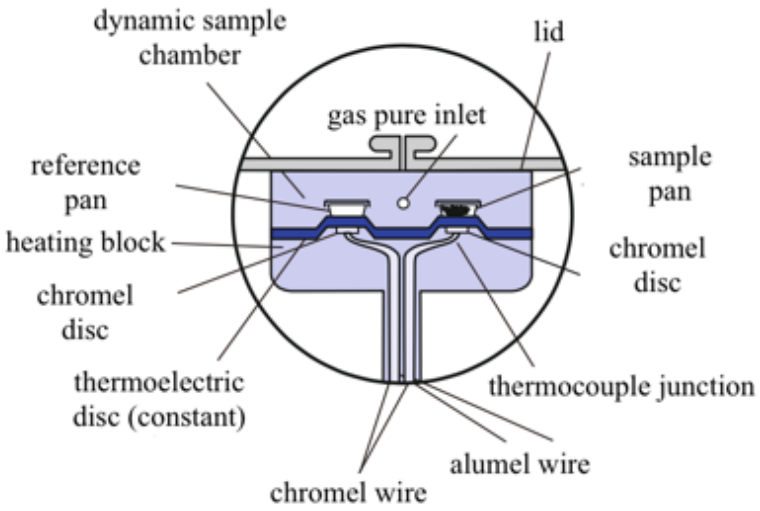

Figure 2.1: DSC measuring cell [10]

The DSC analysis was executed by using a TA-Instruments Q 2000. The instrument was calibrated with an indium standard. The samples were equilibrated by -50°C then held isothermal for 5 minutes and then heated up to 250°C with a heating rate of 10 K/min. At 250°C the temperature was held for 1 min and then cooled down to -50°C again with a heating rate of 10 K/min. After an isothermal stage for 5 minutes and another heating run with the same parameters as before were performed.

Table 2.2: Temperature program

Step	Process
1	Equilibre at -50°C
2	Isothermal for 5min
3	Ramp 10 K/min to 250°C
4	Isothermal for 1min
5	Ramp -10 K/min to -50°C
6	Isothermal for 5min
7	Ramp 10 K/min to 250°C

2.1.2 TGA

Thermogravimetric analysis (TGA) is another important tool for polymer characterization. The method measures mass changes of a sample as a function of time and or temperature. Evaporation, decomposition, oxidation or other chemical reactions are resulting in a loss of mass which is measured with TGA. A microbalance is positioned in an oven. In this oven, a defined atmosphere is provided. This atmosphere can be inert (N_2) or oxidizing (Air). While the device is performing the temperature/ time program, the weight of the sample is measured. From the plotted graph, conclusions can be drawn on the degradation kinetics of the tested sample. [10]

The thermal stability of PA 6 and aramid was determined by using a TA-Instruments TGA 2050 under nitrogen and air flow. The PA 6 samples with a weight of 5mg ± 10% were heated up to 600°C with a heat rate of 10 K/min. Before heating they were held by room temperature for 1 minute. The aramid samples were heated with a heat rate of 10 K/min up to 700°C also with an isothermal phase of 1 minute by room temperature.

Sample Preparation

For both DSC and TGA analysis the cross-section of the inner pipe was divided into 5 sections (A-E) for sample taking. See figure 2.2. The jacket was divided into 3 sections (in-(A), outside(E), middle(C)). From each section, a slice with a thickness of 200µm was cut down with a rotary microtome Mikrom HM 360 and cropped into pieces of 3mg for DSC and 5mg for TGA.

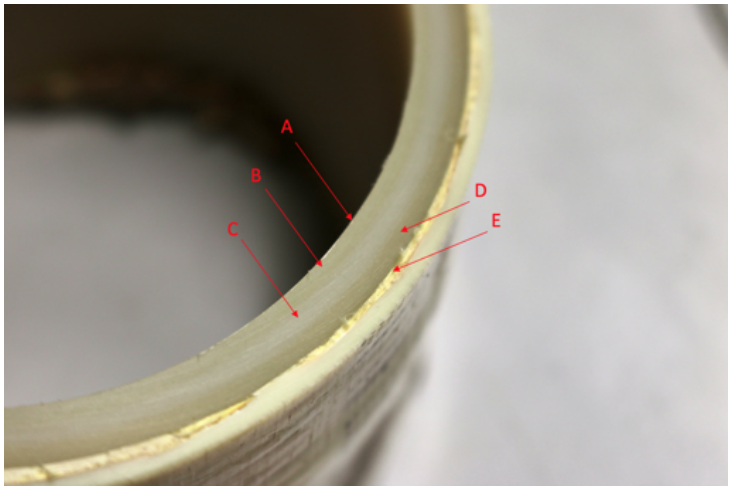

Figure 2.2: Division of the cross section

2.2 Mechanical Analysis

2.2.1 Tensile Test PA6

With the tensile test, the tensile strength behaviour of a material can be determined. The fact that the test is quite easy to execute and that it provides a lot of informative material parameters like Young's modulus, yield stress, tensile strength, tensile stress at break and the corresponding strains, tensile tests are a good option for material classification. It is a quasi-static test where a uniaxial loading and stress in the specimen should be generated. The specimen is fixed between two clamps. The tensile force, which must be applied without impact and increased slowly, is applied to it until the specimen cannot retain the force anymore and fracture occurs. During the test, force and changing in length is measured. While the cross-section A is changing during the experiment, tensile stress is calculated with the initial cross-section A_0 according to formula 2.1. Elongation is related to the initial gauge length L_0.

$$\sigma = \frac{F}{A_0} \tag{2.1}$$

$$\epsilon = \frac{\Delta L_0}{L_0} * 100\% \tag{2.2}$$

Typical stress-strain diagrams of various plastics with material defining values are shown in figure 2.3:

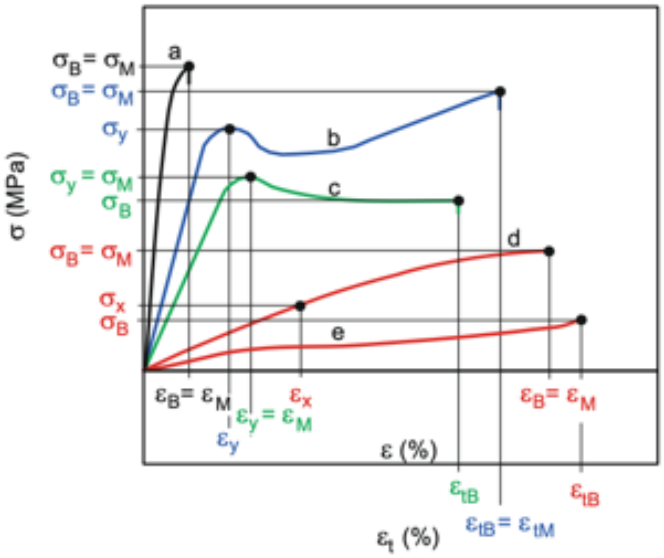

Figure 2.3: Various stress-strain curves [10]

Parameters according to ISO 527:

- Yield stress σ_y
- Tensile strength σ_M
- Stress σ_x a x% of strain
- Tensile stress at break σ_B
- Yield strain ϵ_y
- Strain at tensile strength ϵ_M
- Tensile strain at break ϵ_B

Graph a shows a brittle material behaviour with high tensile strength σ_M and a tensile strain at break ϵ_B up to 10%. Typical representatives of this material behaviour are Polystyrol (PS), brittle thermoplastics, duroplastics as well as filled and reinforced plastics.
The Graphs b, c and d are corresponding to ductile deformation behaviour with

tensile strain at break of several hundred percent. The tensile strength is relatively small. Polyolefines and Polyamides are plastics with this material behaviour.
A material with low tensile strength and Young‘s modulus is shown in graph e. The tensile strain at break can be up to 1000%. PVC-P, synthetical and natural rubber are assigned to this group of plastics. [10]
The conditioning is playing a decisive role in the deformation behaviour of PA. The more water is absorbed the flatter the curve gets. This means that tensile strength and Young‘s modulus are decreasing whereas the tensile strain at break increases. This behaviour can be seen in figure 2.4. For dry PA6 the stress-strain curve shows a brittle material behaviour with high Young‘s modulus. For PA6, stored under a relative humidity of 75%, the tensile strength is about a quarter of dry PA6. According to figure 2.5, a relative humidity of 75% corresponds to a water-content of 6,5% weight of the PA6. It is also clearly evident, that with increasing humidity the gradient and therefore Young‘s modulus is decreasing.

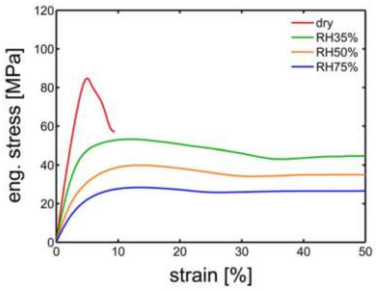

Figure 2.4: Influence of moisture on PA [12]

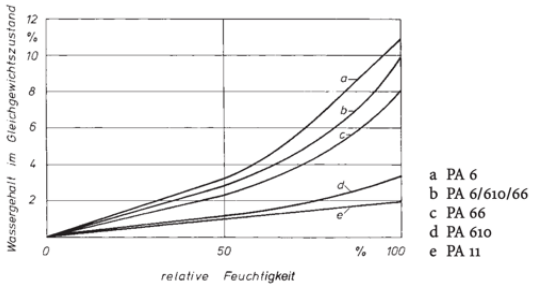

Figure 2.5: Conditioning of PA [9]

Water operates as a softener in PA. At high temperatures, water-free atmosphere and liquids, PA dries out. For avoiding embrittlement, parts for such a use case are often made from a monomer containing PA6. Polyvinyl alcohol (PVAL) and linear polyurethane (TPU) have a similar softening effect as water. [9]

To determine the tensile stress at yield and Young‘s modulus a Zwick Roell Z050 with a 10kN load cell were used. As testing speed was chosen v=50 mm/min for the PA 6 samples. For testing the standard specification specimen, a Zwick Roell Z250 with a 250kN load cell was used.

2.2.2 Tensile Test Aramid

The aramid yarn could not be tested according to DIN EN 12562 because there was not enough yarn available as requested. Also the clamp type needed for the test was not accessible. So the tensile test for the Aramid yarn was carried out with a modified test setup. For the tensile test, 20cm of the aramid yarn was extracted from the textile to be twisted around two aluminium cylinders with a diameter of 10mm. The yarn was thread through a hole with a diameter of 2mm and fixed with a knot. Afterwards, the yarn was wounded around the cylinders until it was streched. The cylinders were then fixed between the clamps. The testing speed for the aramid fibres was v=10 mm/min.

2.2.3 Charpy Notched Impact Test

The impact toughness of plastics or other materials can be determined with the Charpy impact test. For the test, a pendulum hammer with a defined energy and velocity impacts on a specimen with three-point support. When the hammer breaks the specimen and keeps on rotating, the maximum of the remaining deflection, which is proportional to the lost energy, of the hammer is measured. [10]
By creating a stress concentration through a notch, even very tough materials which would not break when unnotched, will break through. The impact toughness a_{cN} [J/m^2] can be calculated with formula 2.3. W_c [J] is the corrected work taken to break the specimen, b_N [mm] is the residual width and h [mm] is the thickness of the specimen.

$$a_cN = \frac{W_c}{b_N * h} * 10^3 \tag{2.3}$$

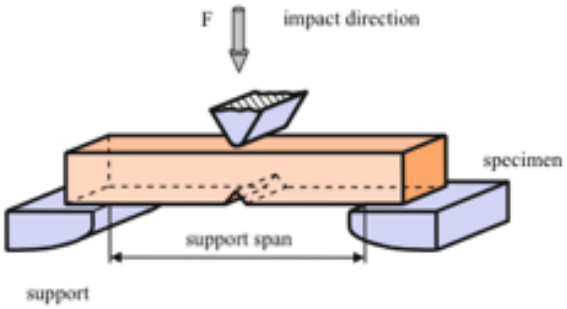

Figure 2.6: Charpy notched impact test arrangement [10] edited

Except for the sample geometry, the test was carried out according to ISO 179-1, edgewise impact with notch shape A. A 25J Charpy hammer according to ISO 13802 was used for the Impact test.

Sample Preparation

For the tensile test specimen, stripes with a length of 120mm were cut lengthwise out of the pipe material with a band saw, as shown in 2.7, and ground to a thickness of 2mm.

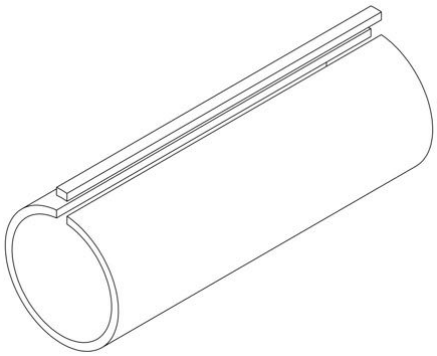

Figure 2.7: Pre-cut of tensile test specimen

It turned out that the specimen cannot be tested properly because they got pulled out of the clamps of the testing machine. So a section at a length of 50mm in the middle of the specimen was grounded to a thickness of 1mm. This is shown in figure 2.8.

For a repeated testing standard specification specimen of type 1B according to ISO 527-2 was cut out with a water jet cutter.

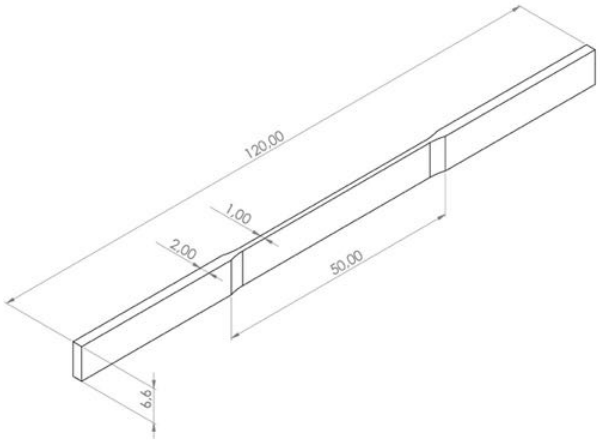

Figure 2.8: Tensile test specimen

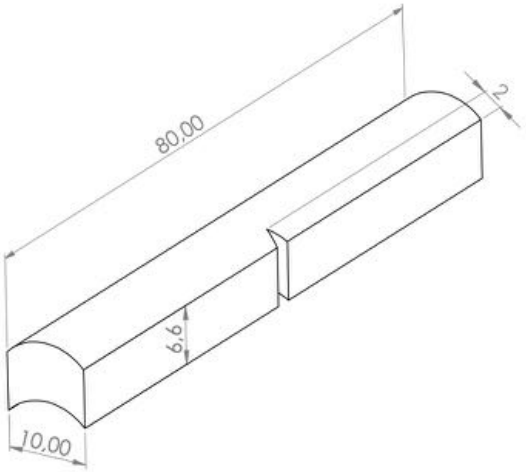

Figure 2.9: Notched Charpy impact test specimen

The test specimen used for the Charpy notched impact test was cut out of the pipe lengthwise with a length of 80mm and a thickness of 10mm. A 2mm deep notch was planned with a Ceast Notch-Vis notch device. A sketch of the specimen is shown in figure 2.9

Figure 2.10: ISO 527-1 1B specimen

Figure 2.11: ISO 527-1 1B specimen

In figure 2.10 and figure 2.11 a standard specification specimen according to ISO 527-1 1B can be seen. The bend which can be observed in figure 2.11 comes from the reel, the pipes were coiled up.

2.3 Optical Analysis

2.3.1 FTIR

Infrared spectroscopy (IR) in plastics engineering is used for material identification of unknown samples and quantitive determination of known substances. After the measurement, the received spectra are compared to spectra of IR libraries and act as a kind of "fingerprint". In figure 2.12 the configuration diagram of an FTIR spectroscope can be seen. If infrared light is thrown on the sample, the functional groups are reacting with characteristic vibration. This can be either valence vibration or deformation vibration. The absorption spectrum is created due to this interaction. Normally infrared light with a wavelength of 2,5 – 25μm, which equates to a wavenumber of 4000 cm^{-1} to 400 cm^{-1}, is used. In material analysis, Fourier transformation infrared spectroscopy (FTIR) is used nowadays. A special measuring procedure is the attenuated total reflection (ATR) where the light is not shining through the sample. The two different indices of refraction of a diamond and the sample are used for ATR. Only in a small area, the IR light is penetrating the sample stimulating vibrations of molecules. [13]

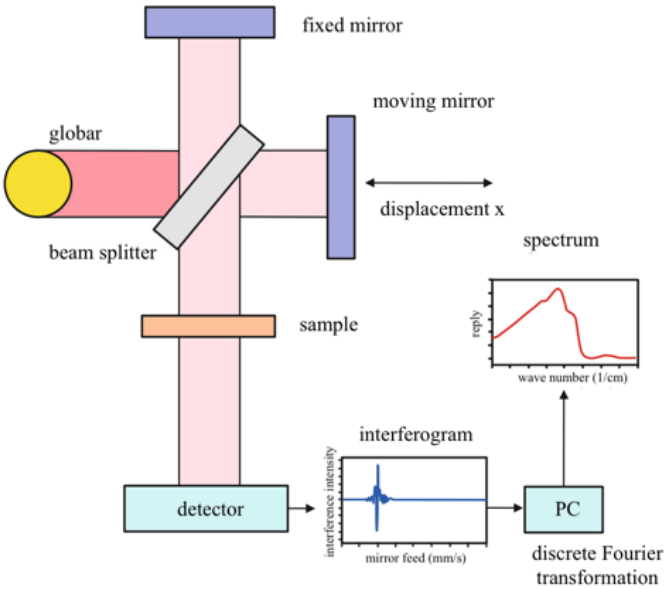

Figure 2.12: FTIR operating mode [10] edited

A Brucker Hyperion 1000 spectroscopy microscope was used for the FTIR analysis. The measurements were carried out using the ATR mode in a frequency range from 4000 cm^{-1} to 400 cm^{-1}.

Sample Preparation

For FTIR analysis the wall thickness was divided into 14 sections (a-n), similar to the procedure of the sample preparation for the thermal analysis. Sample a was taken from the inner surface, n from the outer surface of the liner, the others between them. The resolution between the sample taking points is given in table 2.3.
Slices with a thickness of 30μm were cut for the FTIR analysis with a rotary microtome Mikrom HM 360.

Table 2.3: Resolution of the FTIR analysis

Sample	Resolution [μm]
a-e	100
e-j	1000
j-n	100

2.3.2 EDX

With energy disperse X-ray spectroscopy chemical characterization of samples can be carried out in a non-destructive way using a scanning electron microscope (SEM). The X-rays with specific energies for each element, generated by irradiation of the sample with an electron beam of uniform energy, give information of the composition of the sample. The electron beam fired on the sample knocks out electrons of the inner shell of atoms and the vacancies are filled with atoms of the outer shell. By this interaction, x-ray beams which energy corresponds to the difference of the energy state in the two shells, are emitted. This x-ray beams can be assigned to the elements in the sample because every element has its characteristic radiation. The intensity of the signals gives information about the amount of each element too.[14]

For the EDX analysis, an FEI Philips XL 30 scanning electron microscope with a connected energy dispersive microanalysis system was used. As sputtering unit an Agar Scientific Agar Sputter Coater B7340 was used.

Sample Preparation

For the EDX investigation, a piece of the pipe was cooled down to ≈ -196°C with liquid nitrogen to broken and to obtaining a smooth fracture surface. The fracture surface was then steamed with gold to become electrically conductive.

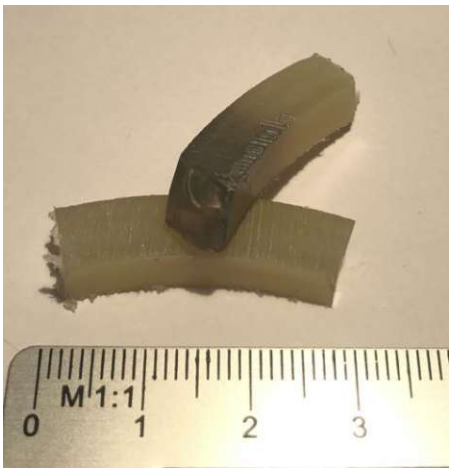

Figure 2.13: Gold-coated cryobreak

2.3.3 Dye Penetrant Test

A dye penetrant test was carried out with the jackets to find out how deep the cracks penetrate the material. For this test, a special dye penetrant inspection colour which is usually used for the inspection of welding lines was applied on the surface.

3 Results

After a visual examination it was seen, that massive damage occurred on the outside of the Jacket. Numerous micro-cracks as shown in figure 3.1 could be identified. The type of fracture was to be determined on every single piece of the four pipe fragments. Not only the jacket was affected, but also the liner exhibited similar cracks as it can be seen in figure 3.2.

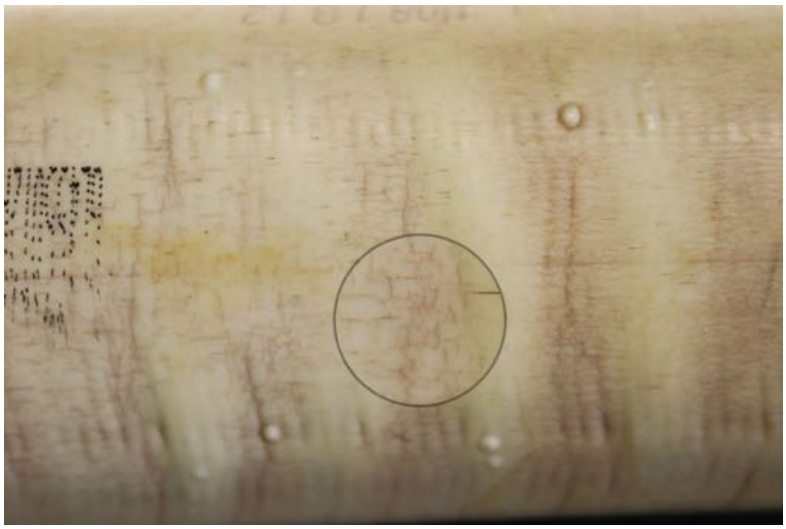

Figure 3.1: Jacket

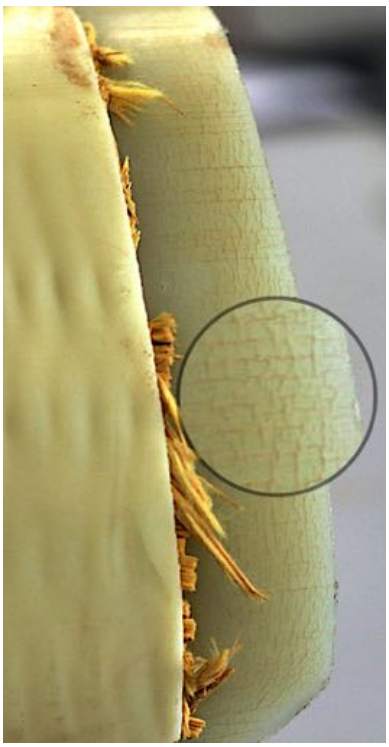

Figure 3.2: Aged end of pipe 1

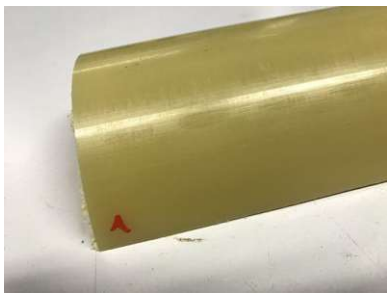

Figure 3.3: Uncovered liner of pipe 1

After removing the jacket and the aramid textile, it was found that the apparent damage of the liner was only present at those areas where the liner was not covered with the textile and the jacket, i.e. at the four endings of the pipes. The uncovered liner is shown in figure 3.3.
For the investigation of the jacket with the dye penetrant test, the colour was applied on the surface of the jacket as it is shown in figure 3.4. After the colour was dried, the cross-section of the specimen was sanded and investigated under a microscope. As it can be seen in figure 3.5, the cracks are infiltrating the jacket by approximately a third of the wall thickness. This observation was made on each of the four pipes. A dye penetration test for the liner was not applied because it did not exhibit fracture at the jacket- covered areas.

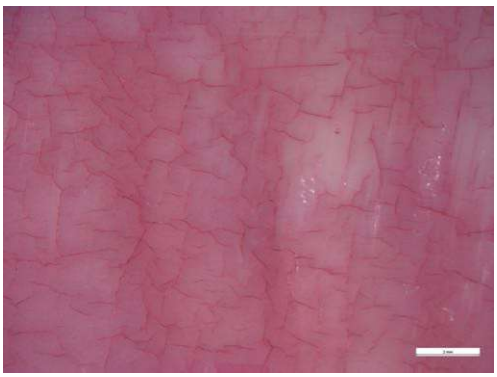

Figure 3.4: Color penetration testing

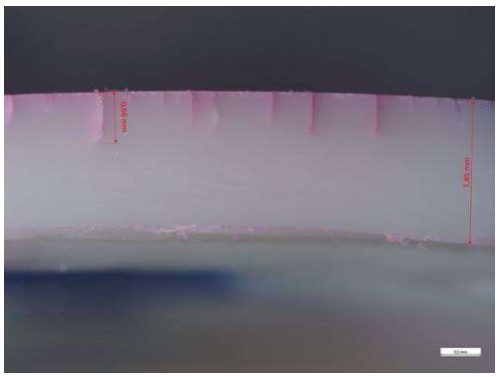

Figure 3.5: Depth of cracks

A cross sectional view of the lining material shows three different layers, which can be seen in figure 3.6. The inner and outer layers of the liner are darker than the brighter middle layer. The initial idea was that the variation of the colours was caused by the production process of the liner and it might be a variation of the crystallinity. For further assessment, the composition of the material had to be first analysed.

Figure 3.6: Cross section

3.1 DSC

Figure 3.7 illustrates the behaviour of the melting temperature T_m of the liner material over the wall thickness of the liner. It can be seen that the melting temperature on the inside (measuring point A) of the pipe is approximately at a value of T_m=217°C. At the three inner measuring points (B, C, D) the temperature of melting is sinking to T_m=215°C. On the outside (E) it is T_m=217°C again.

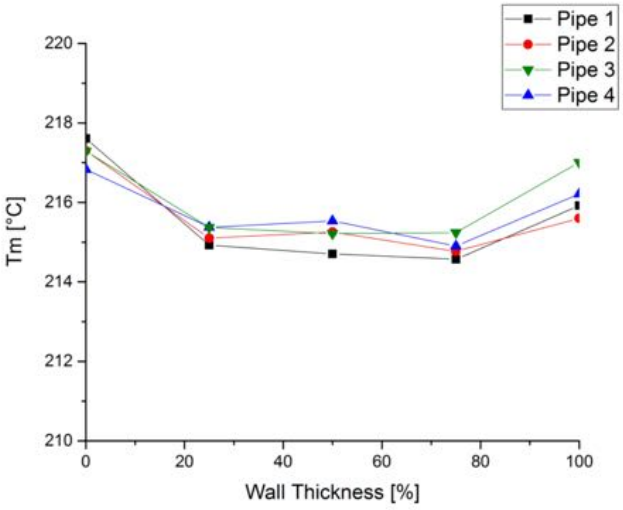

Figure 3.7: Melting temperatures

This confirms that the liner of the RTP consists of PA6. Domininghaus [9] gives a melting temperature for PA6 of T_m=220°C which correlates quite well to the values of the DSC analysis. The difference in the melting temperature of the inside and the outside of the liner can be either caused by the various crystalline structures of PA6. This is the α- and γ- phase and the amorphous δ- phase. Another possibility are the diverse reactions of the PA6 to the environmental conditions. It is evident that the two outer layers (A, E) are forming a significant second melting peak as shown in figure 3.8. The inner layers also show this kind of behaviour but not so obviously. This second peak does not only appear at pipe 2, but at all other 3 pipes.

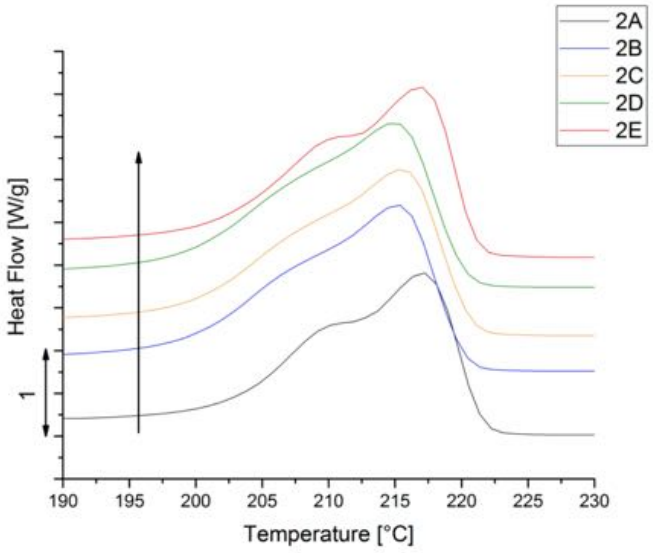

Figure 3.8: Melting peaks of pipe 2 with offset

As [9] says the crystallinity of PA6 is about X_c=35% - 45%. According to [15] the crystallinity is calculated after formula 3.1 where H_m [J/g] is the melting enthalpy and H_0 [J/g] is the melting enthalpy of 100% crystalline PA6.

$$X_c = \frac{\Delta H_m}{\Delta H_0} * 100 \tag{3.1}$$

For H_0 a value of 190J/g was chosen according to [15] and [16]. In figure 3.9, where the degree of crystallinity is printed over the wall thickness, one can see that the degree of X_c is in the area [9] is pretending for PA6 with a little variation, especially on the inside. Even the crystallisation temperature which is given with T_c=188°C [17] for PA6 is variating and it is again higher on the in- and outside than it is in the middle of the liner. As it can be seen in figure 3.10 crystallisation starts earlier on the in- and outside of pipe 2, whereas the peak of B, C and D is at the same temperature. This behaviour can be observed at all four pipes as it is illustrated in figure 3.9.

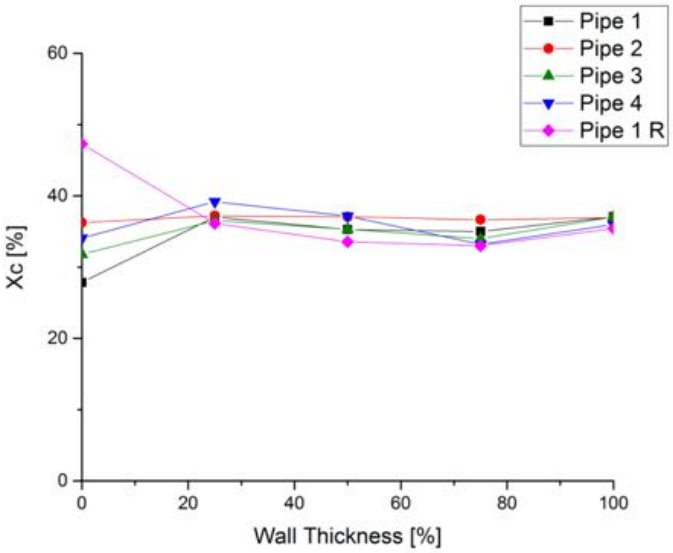

Figure 3.9: Crystallinity

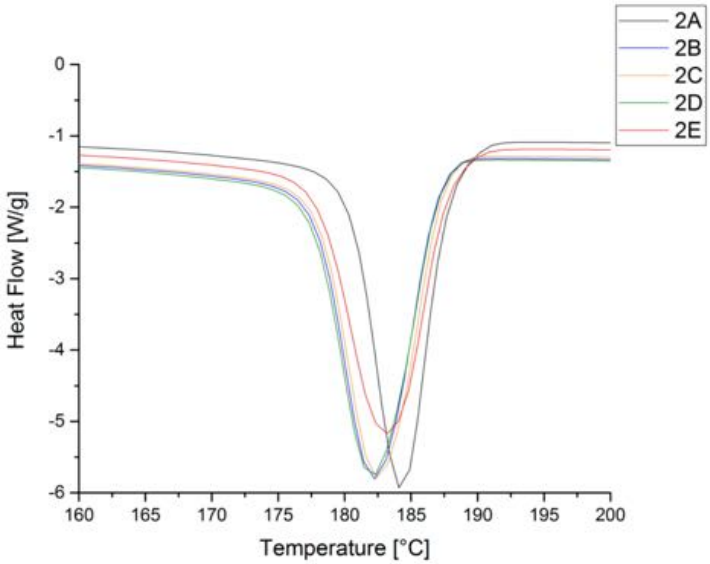

Figure 3.10: Crystallization peaks of pipe 2

Figure 3.11 illustrates the crystallization temperature of the single pipes across the cross-section. It can be seen that the temperature varies a little bit from the outside to the inside. Only sample Pipe 1 R, which is taken from the aged area at the edge of pipe 1, has a wider range of variation with Δ T_C=5°C.

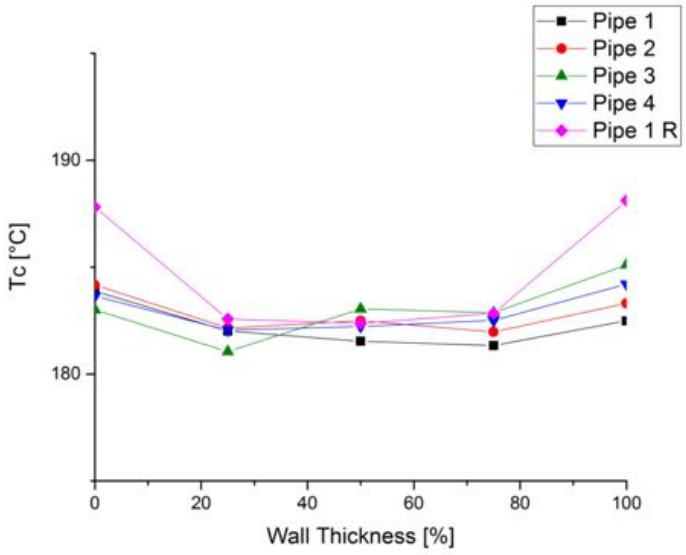

Figure 3.11: Crystallisazion temperature

In figure 3.12 the melting peaks of the aged area on the edge of pipe 1, shown in figure 3.2, are recorded. The graphs of B, C and D show the same behaviour as the graphs of the other samples which were covered with the jacket. The double peaks of the two outer samples A and E are much more distinctive. At a temperature of approximately 190°C a third peak is forming. This cannot be observed at any other samples. [18], [19] and [16] show that with aging these double peaks become increasingly apparent.
Figure 3.13 compares the melting temperatures of the covered areas with the one of the aged sample. The melting temperature of the inner face of the pipe is exactly the same. With increasing diameter the deviation of the temperature increases to a maximum of + 2-3°C compared to the the aged sample. The difference in crystallinity of the two samples of pipe 1 has its maximum on the inside of the liner. From B to E the course of the two graphs is almost the same.

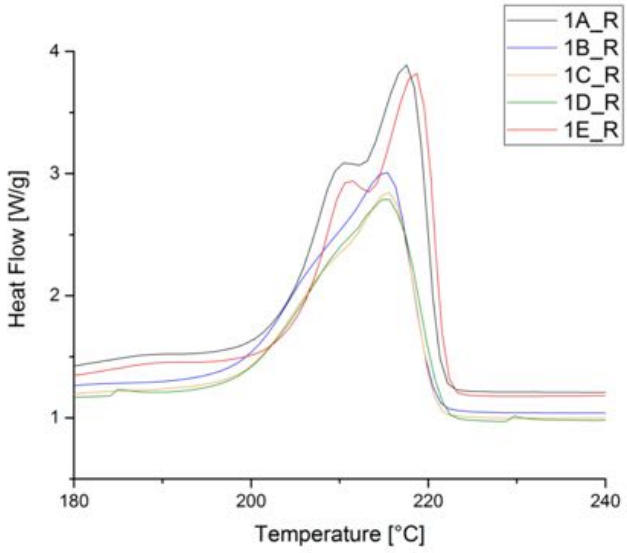

Figure 3.12: Melting peaks from aged area of pipe 1

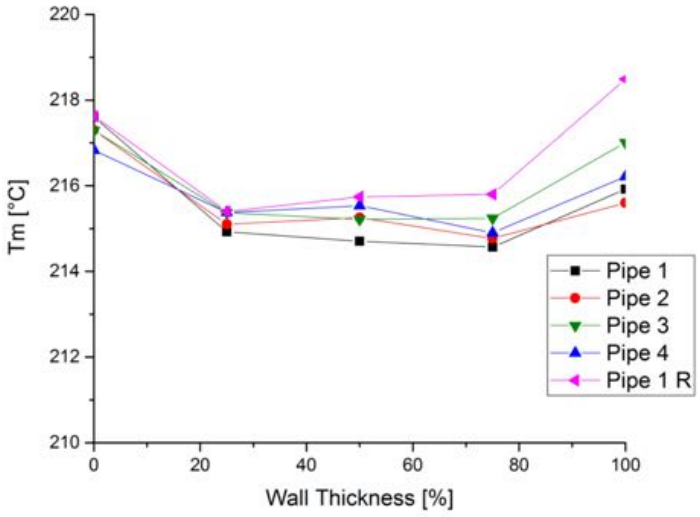

Figure 3.13: Melting temperatures

3.1.1 Jacket

The melting temperature T_m of the jacket indicates that it is also made of PA6. The outside of the jacket shows the same peak as the one of the aged sample from pipe 1. A hint of the peak at 190°C can be seen, too. As the colour penetration testing indicated, the damage on the jacket is limited to the surface, the DSC analysis confirms the suspicion (E). The graphs of the middle and the inside samples of the jacket (A,C) do not point out to any ageing mechanism.

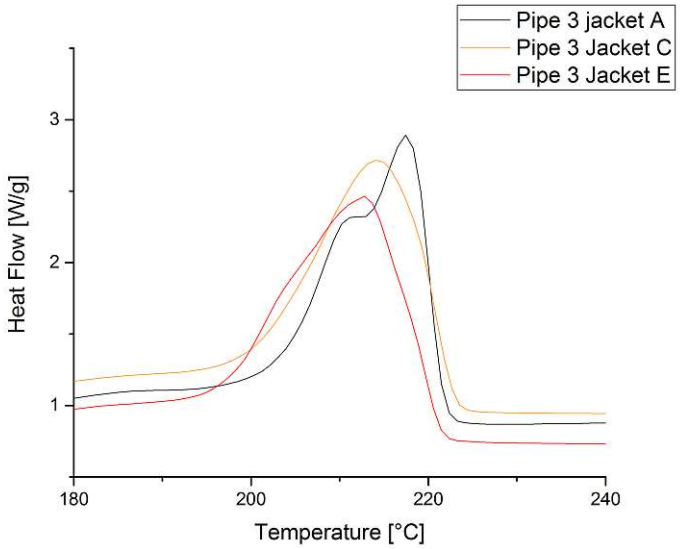

Figure 3.14: Melting peaks of Jacket from pipe 1

3.2 FTIR

The FTIR analysis confirms the hypothesis that the liner material is PA6. In the IR spectra of pipe 1 in figure 3.15 the same peaks can be found as in the spectra in figure 3.16 according to [20] which shows PA6 in different stages of thermal aging. The characteristic peaks are shown in table 3.1 [21].

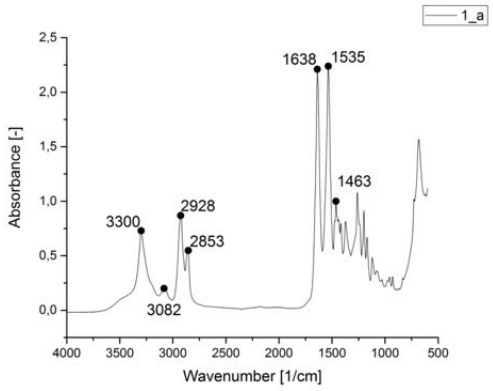

Figure 3.15: FTIR spectra pipe 1

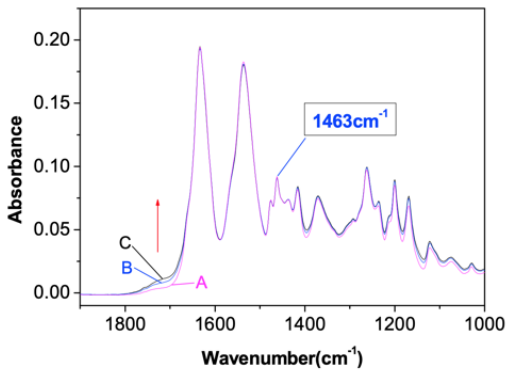

Figure 3.16: FTIR spectra PA6 [20]

Table 3.1: Characteristic peaks

Wavernumber [cm^{-1}]	Peak
1535	Amide II
1638	Amide I
2853	Symmetric CH_2- Streching
2928	Asymmetric CH_2- Streching
3082	Hydrogen bonded NH- Stretching
3300	Hydrogen bonded NH- Stretching

The peak at 1463 cm^{-1} was chosen as reference peak because it is not sensitive to oxidation and therefore it does not change during oxidation [20]. Every measured spectrum was normalized by this peak. At thermo- oxidative aging the IR- spectra changes. [20] proves, that the carbonyl absorbance (1710-1760 cm^{-1}) is increasing by man- made aging at a temperature of 140°C.

The carbonyl band consists of [20]:

- ketones 1715 cm^{-1}
- aldehydes 1725 cm^{-1}
- esters 1735 cm^{-1}
- aliphatic carboxylic acids 1750 cm^{-1}

As it is illustrated in figure 3.16, the carbonyl band is growing in time of exposure. This absorption band of the cross-section of pipe 1 is shown in figure 3.17 where the letters a-n give the position of sample taking. Sample a is taken from the inside, sample n from the outside of the liner. The resolution is given by table 2.3.
A little increase in this area can be observed but no trend is apparent. One would expect that the absorbance was changing in a function of the wall thickness but this is not the case. After investigation of all four pipes, no sample showed any trend at the detected area.

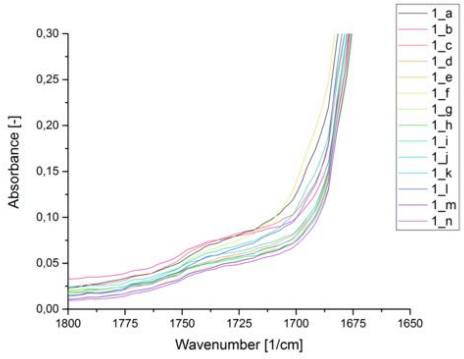

Figure 3.17: Carbonyl group

In [21] the single peaks of the characteristic spectrum for PA6 at unaged samples are visible whereas at samples which are aged for 1600h at a temperature of 90°C – 150°C these peaks are decreasing until they are gone at 180°C. This means that with increasing ageing effects, the peak disappears. CH_2- stretching at a wavenumber of 2930 cm^{-1} and 2860 cm^{-1} and NH- stretching 3295 cm^{-1} was also investigated at the liner samples. As it can be seen in figure 3.18 and figure 3.19 there is a variation in the intensity of the single bands across the cross-section. Again, no trend is obvious and the peaks are far away from an unrecognizable state. This would be the case if massive ageing would have taken place and if the peaks would have been deformed to such an extent that they would no longer be visible.

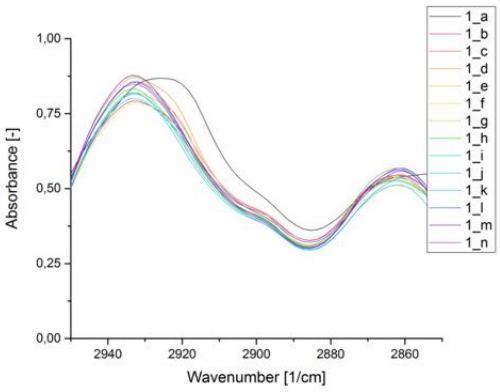

Figure 3.18: CH_2 - Streching

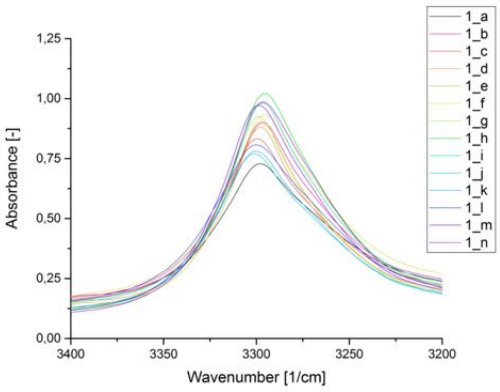

Figure 3.19: NH - Streching

In figure 3.20 can be seen a spectrum of the carbonyl group of sample pipe 1 compared to sample pipe 1 R. It is obvious that the graphs of the aged sample pipe 1 R are shifted up compared to pipe 1. The graphs of pipe 1 are limited to a smaller range, whereas the curves of pipe 1 R are spread wider. Also, a lot of small peaks are arising at pipe 1 R. According to [15] these carbonyl vibrations are an indication of thermal-oxidative ageing. "The methylene groups on the PA6 molecules were oxidized into primary hydroperoxide species, which further decomposed rapidly into carbonyl groups." [15]
A trend within the cross-section of pipe 1 R can not be observed, but it is clear

that the carbonyl region is much more distinctive in the aged sample than in the unaged.

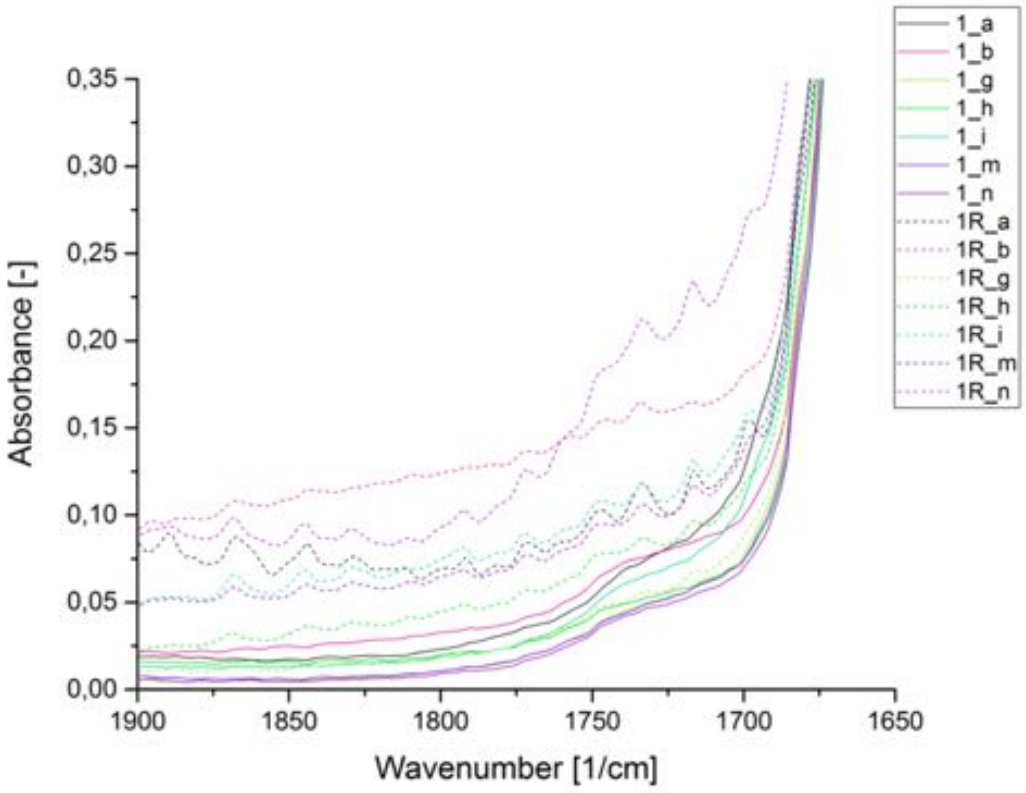

Figure 3.20: Carbonyl group pipe1 and pipe 1R

If CH_2 - stretching at a wavenumber of 2930 cm^{-1} and 2860 cm^{-1} is observed, one can see that de deviation between aged samples 1R and non-aged samples 1 is not as distinctive as at the carbonyl band. Only a shift down from the non-aged samples 1_a and 1_n on the inside at 1R_a and on the outside 1R_n has taken place, which is an indication for thermo oxidative ageing. [15] [21] This behaviour occurs at a wavenumber of 2930 cm^{-1} as well as at 2860 cm^{-1} as it can be seen in figure 3.21 and 3.22. It shows that CH_2 - stretching only occurred on the outside and on the inside of the pipe. The middle layers of the cross-section were spared by this behaviour.

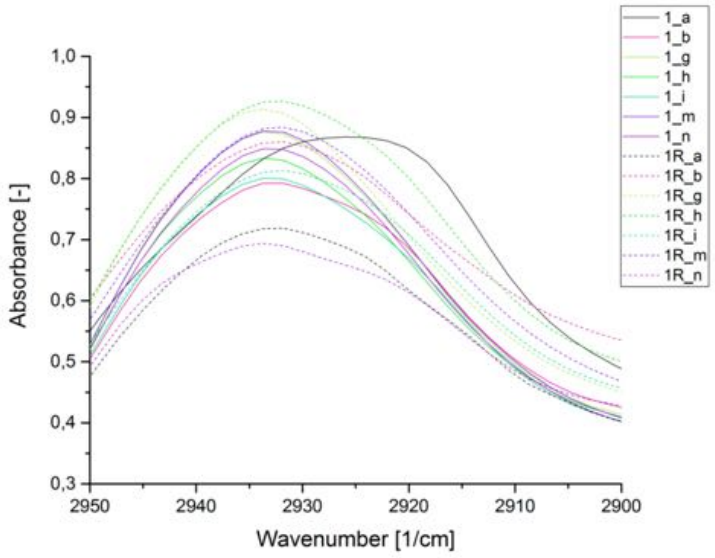

Figure 3.21: CH_2 - Stretching pipe 1 and pipe 1R

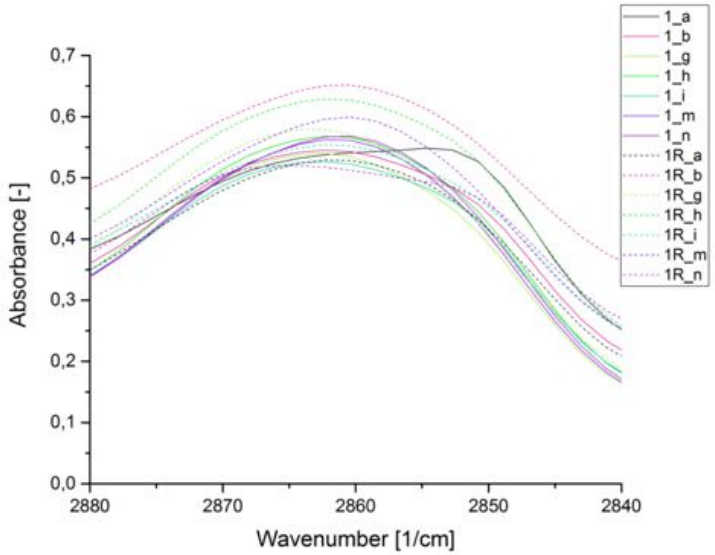

Figure 3.22: CH_2 - Stretching pipe 1 and pipe 1R

Figure 3.23 proves that NH - stretching occurred. A decrease of the curve can be observed for every sample taking point over the cross-section of the pipe which is an indicator for NH -stretching according to [21]. In contrary to the CH_2 - stretching, NH - stretching took place throughout the whole wall thickness of the pipe and not only on the in- and outside.

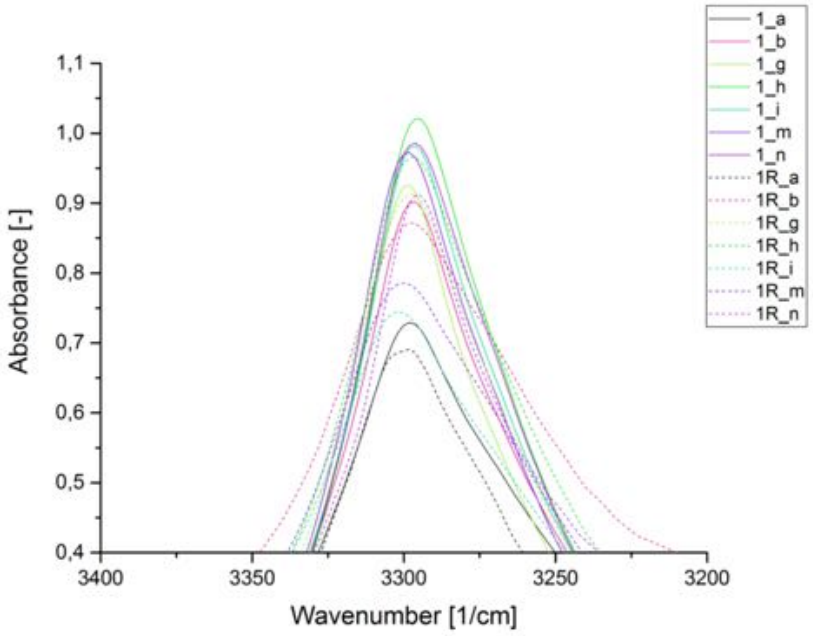

Figure 3.23: NH - Stretching pipe 1 and pipe 1R

The comparison between the textile and jacket covered area of pipe 1 and the uncovered, brittle and probably aged area of pipe 1 R does not allow any statement about the absolute condition of the PA6, because, for this, a reference sample of the material is needed. But it can be said, that if the covered material had been subject to massive ageing, the IR spectrum would not be so different from the one of the ends of the pipes. The spectrum of the carbonyl group shows that the curves of pipe 1 are much smoother and flatter than the ones of pipe 1R.

The next step was to investigate the crystalline composition of the liner material via FTIR which was induced by the three different colours in the cross-section of the liner. Therefore it had to be checked whether the different colourings and thus the presumed different crystalline phases result from ageing. To detect differences in crystallinity of the single layers in the liner, three phases were investigated with the peaks and a new reference peak according to [19]. This paper gives also a new reference peak at 1170 cm^{-1}.

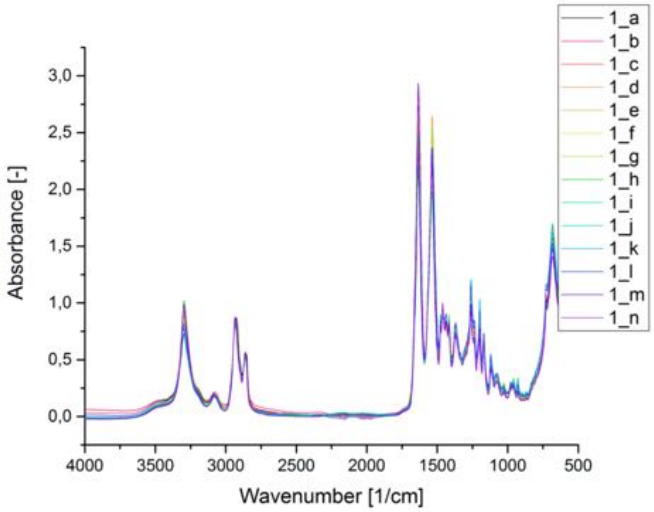

Figure 3.24: FTIR spectra

- reference peak
  - 1170 cm^{-1}
- amorphous δ- phase
  - 1124 cm^{-1}
- hexagonal γ- phase
  - 975 cm^{-1}
- monoclinic α- phase
  - 930 cm^{-1}

It was expected, that in the supposedly three different layers of the liner which are discernible by different colours, displayed in figure 3.6, show various crystalline structures. An increase in the intensity of the absorbance of the above- mentioned peaks would mean a higher amount of the peak belonging phase.
As in figure 3.25 diagrammed, the peak at 1124 cm^{-1} representing the amorphous δ - phase, does not show any correlation to the position where it was taken from. There is a variation in the absorbance over the cross-section as it can be seen in figure 3.26 but it does not give any reasons for the different colourings.

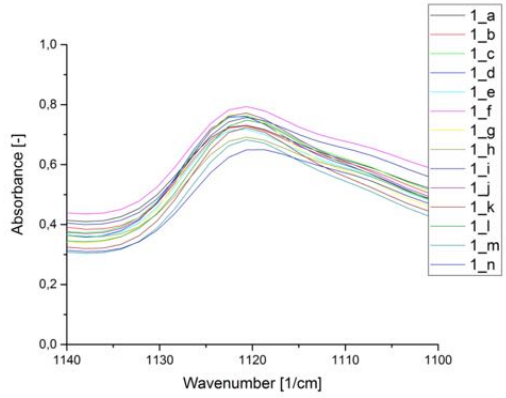

Figure 3.25: Amorphous phase

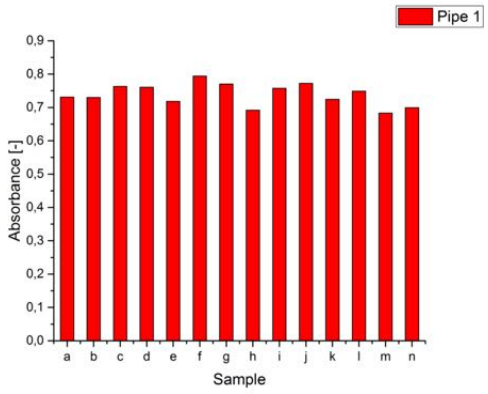

Figure 3.26: Intensity at 1124 cm^{-1}

A similar situation can be observed with the hexagonal γ - phase. The distribution of the intensity of the peak at 975 cm^{-1} does not give any information about the changing in crystallinity. Figure 3.27 shows, that the distribution of the γ - phase is equal over the wall thickness.

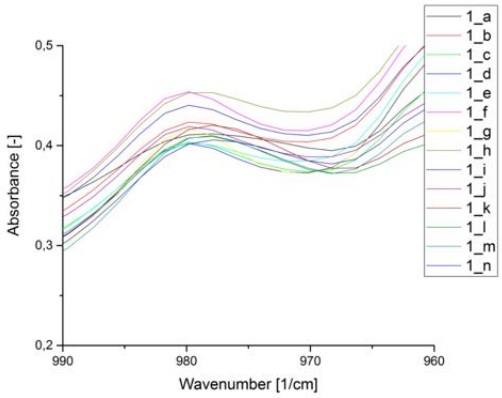

Figure 3.27: Hexagonal phase

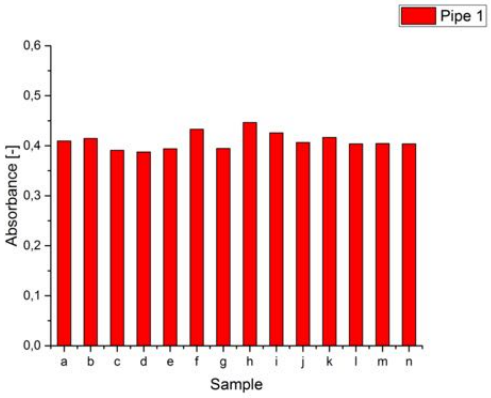

Figure 3.28: Intensity at 975 cm^{-1}

Only the monoclinic α - phase shows a slight downward trend. The intensity of the absorbance decreases with an increasing diameter as it can be seen in figure 3.30. The outer 5 samples are representing a thickness of 0,5mm of the wall thickness according to 2.3. The thickness of the various layers of the different colourings is approximately 2mm. Therefore no direct correlation between the downward trend of the monoclinic α - phase and the different colouring is possible.

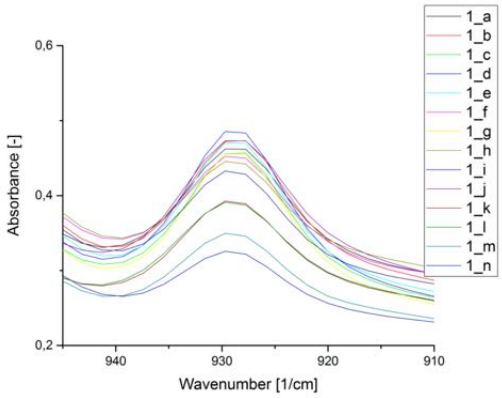

Figure 3.29: Monoclinic phase

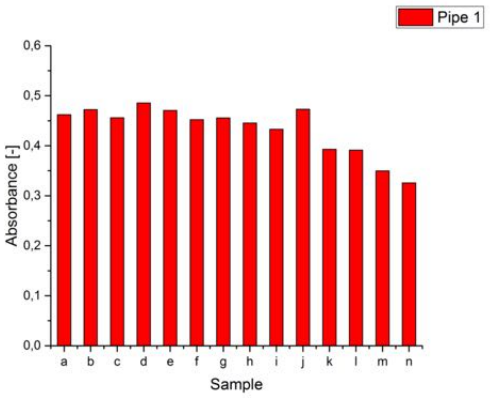

Figure 3.30: Intensity at 930 cm^{-1}

3.3 TGA

The TGA was carried out to examine the degradation behaviour of the polyamide. The first thing to observe is the step at approximately 200°C, shown in figure 3.31. The assumption was that it comes from the water the PA6 has absorbed during its storage. According to [9] this is 2,5% - 3,5% at normal climate of 50% relative humidity and 23°C in which the samples have been stored. To check this thesis, the TGA samples were heated to 100°C at a rate of 10K/min and held for 2h at this temperature. Afterwards, the heating process was carried on to 600°C. The results show, that after 2h the weight loss was only 3% which correlates to the data provided by [9].

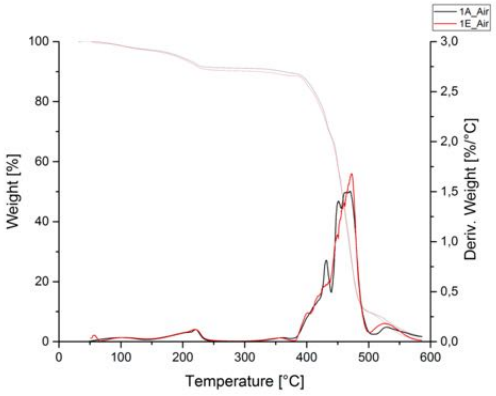

Figure 3.31: TGA curve pipe 1 air

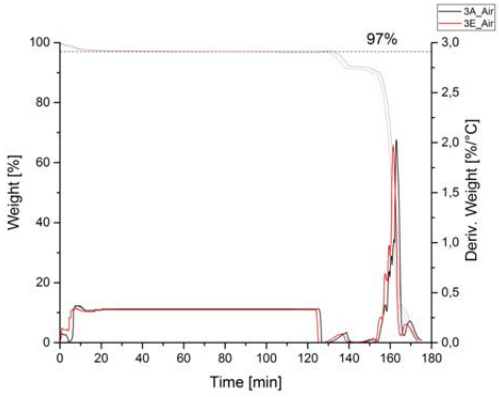

Figure 3.32: Waterstep pipe 3 air

This means that another substance is decomposing at 200°C. As [22] shows, pure PA6 does not have such a step in it's TGA curve, which means again, that the liner material must contain fillers. For this reason the mass at a temperature of 300°C, m_{300} was investigated. As a reference, samples from the obviously aged material at the age of pipe 1, shown in figure 3.2, were taken and compared to the other samples which were protected by the textile and the jacket. As it can be seen in figures 3.34, 3.35 and table 3.2 the values for m_{300} vary by maximum 3% between the middle of the liner and the outside. The values appear in the same order of magnitude for both, air- and nitrogen- atmosphere. For the samples from the aged

area, a different picture emerges. The mass difference between the middle and outer layer is significantly higher. The order of magnitude for both atmospheres is the same again, but the mass differs about 8%. In the outer regions of the aged area, the filler is either decomposed or has evaporated during the lay-days. The same concentration is found in the middle of the aged and the unaged material.
For the evaluation, two specific temperatures were analysed both in air and in nitrogen atmosphere. The first temperature is T_{maxdeg} where "maxdeg" stands for maximum degradation. It is the temperature, where the TGA curve shows the highest gradient and therefore it is the temperature where the degradation is on a maximum. The second temperature is $T_{3\%step}$. As it can be seen in figure 3.33, $T_{3\%step}$ is defined at 3% weight under the prominent point at which strong degradation begins.

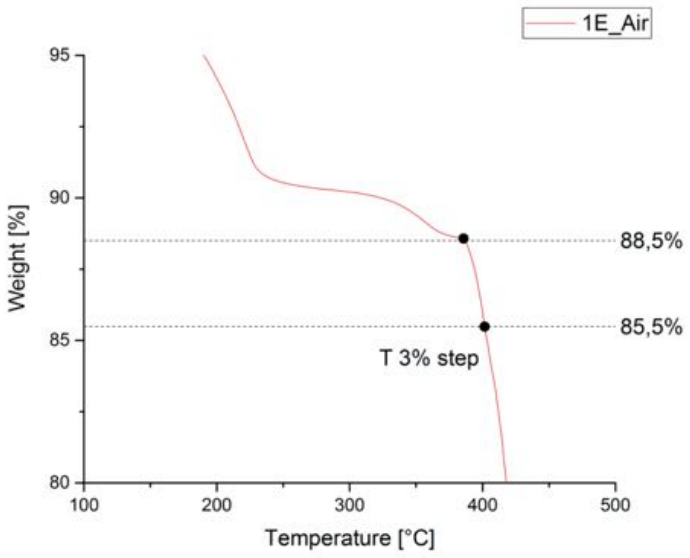

Figure 3.33: 3% step

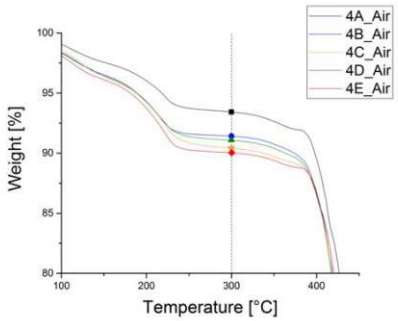

Figure 3.34: T_{300} pipe4 air

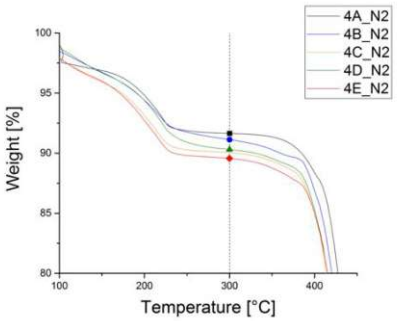

Figure 3.35: T_{300} pipe 4 N_2

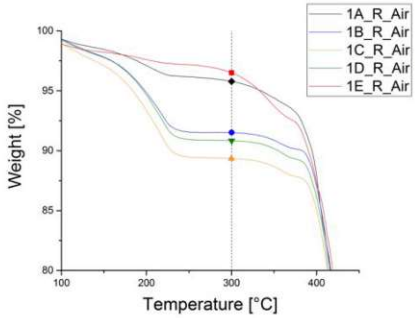

Figure 3.36: T_{300} pipe 1 R air

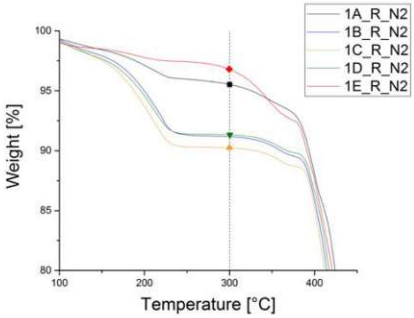

Figure 3.37: T_{300} pipe 1 R N_2

Table 3.2: m_{300} pipe 4 unaged

	Pipe 4 Air	Pipe 4 N_2
Sample	[%]	[%]
A	93	92
B	91	91
C	90	90
D	91	90
E	90	90

Table 3.3: m_{300} pipe 1 aged

	Pipe 1 Air	Pipe 1 N_2
Sample	[%]	[%]
A	96	96
B	92	91
C	89	90
D	91	91
E	97	97

In figure 3.38 and figure 3.39 the overlay of a TGA and a DTG curve is shown. One can see that degradation starts earlier at sample 1 R. This is the case if 1A R is compared with 1A and 1E R with 1E.
In figure 3.40 and figure 3.41 the course of the beginning of degradation across the cross-section of all four pipes is displayed. In both atmospheres, air and nitrogen, the degradation starts at about 400°C. For the aged sample 1 R, the degradation starts earlier on the in- and the outside of the pipe. The deviation in $T_{3\%\ step}$, where degradation begins, between 1 R and the other samples is approximately 5°C for the in- and the outside (A, E) of the pipe. For the three taking points B, C, D in the middle of the pipe, the degradation behaviour seems to be the same for aged and non-aged samples pipe 1 R and pipe 1.
In [23] is shown that degradation starts earlier after exposure to UV radiation. The point where degradation starts moves to lower temperatures. This means that the thermal stability of the brittle end is less than in the covered areas.

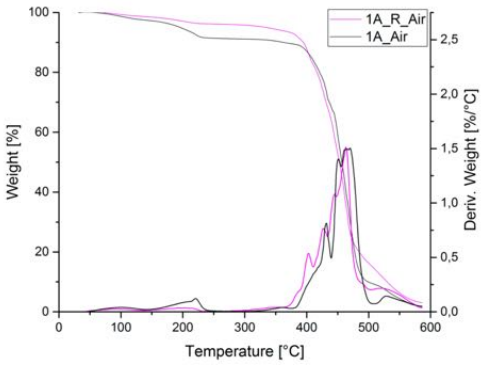

Figure 3.38: TGA/DTG A

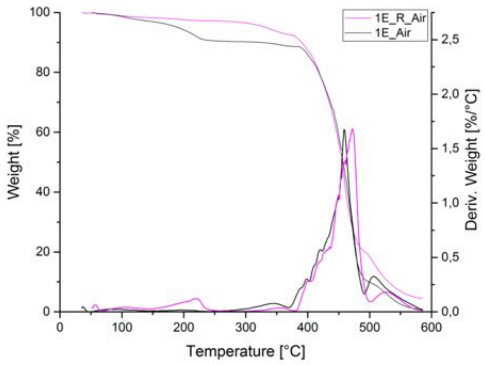

Figure 3.39: TGA/DTG E

The divergence between aged and non-aged samples is in the range of the fluctuation of the single samples as it can be seen in figure 3.40 and 3.41.

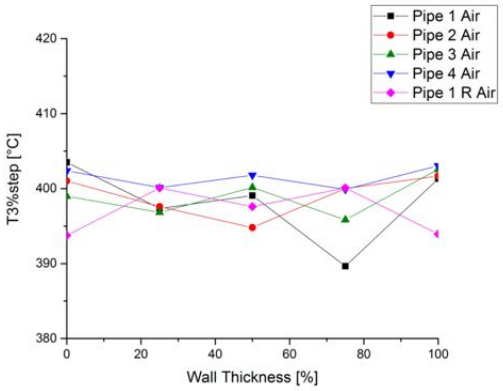

Figure 3.40: $T_{3\%\ step}$ air

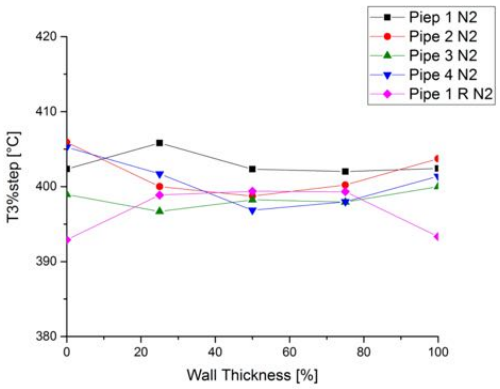

Figure 3.41: $T_{3\%\ step}$ N_2

The point of maximum degradation can be seen as a peak in the DTG plots 3.38 and 3.39. T_{maxdeg} on in- and outside of pipe 1 R is lower than in the unaged areas of the pipes. In the middle, T_{maxdeg} of 1 R is about 10°C lower than in the other samples. If figure 3.43 is observed, one can see that the remaining mass of 1 R, when degradation is on a maximum, is higher in the middle of the pipe than at the other samples.
Here again, no significant deviation from the aged specimen to the non-aged specimens can be detected.

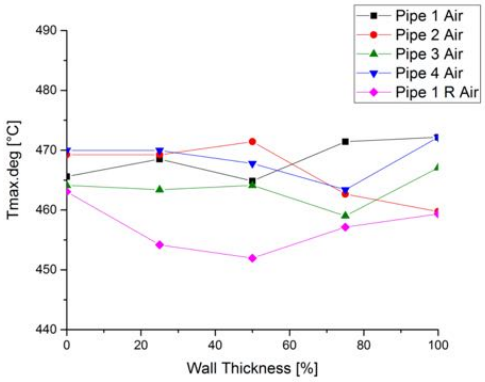

Figure 3.42: T_{maxdeg} air

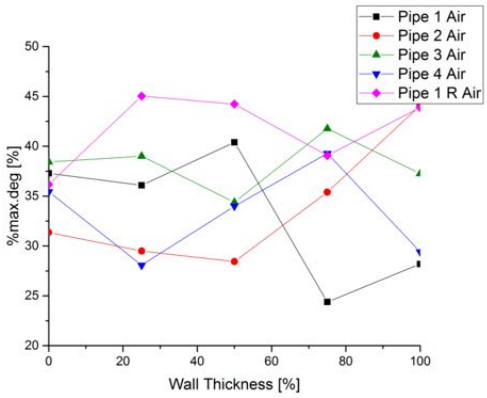

Figure 3.43: m_{maxdeg} air

3.3.1 TGA Aramid

Since no reference samples were available for the evaluation of the TGA curves of the reinforcement, shown in figure 3.44 and 3.45, three characteristic points according to [24] were used. These points are:

- $T_{firstdeg}$: onset of weight loss
- $T_{strongdeg}$: onset of intensive decomposition
- $T_{4\%}$: 4% weight loss

Two eye-catching steps can be seen in the TGA curves. The first one at about 150°C was suspected to come from the water, which the Aramid fibres have taken up. For Twaron saturation is reached at 5,7% according to [25]. Analysis showed that the weight loss at the first step is about 3-4% which strengthens the thesis that the step is evoked by water.
The second step can not be observed in [24] but the degradation begins almost at the same temperature as in the reference values in table 3.4. The temperature, where strong degradation begins in the fibres is also just about 10°C lower than at the reference samples.
Only the values for $T_{4\%}$ deviate from the reference values. For better comparability, $T_{4\%}$ is taken at 4% under the step where all water is evaporated. The deviation to the reference values is here more than 150°C. It is not indicated in [24] whether the fibres were conditioned or not, but no water step is visible in the curves.

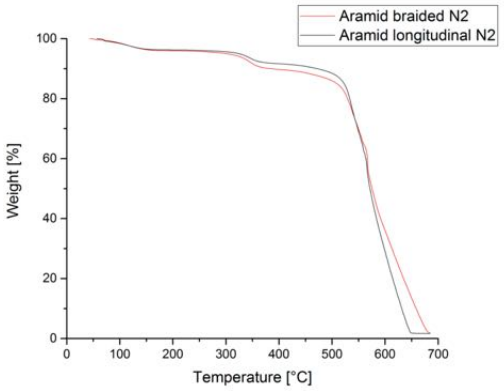

Figure 3.44: TGA Aramid under N_2

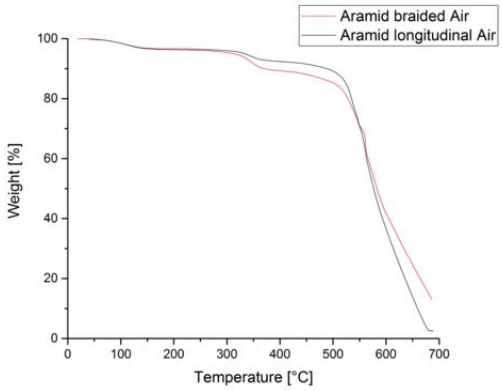

Figure 3.45: TGA Aramid under Air

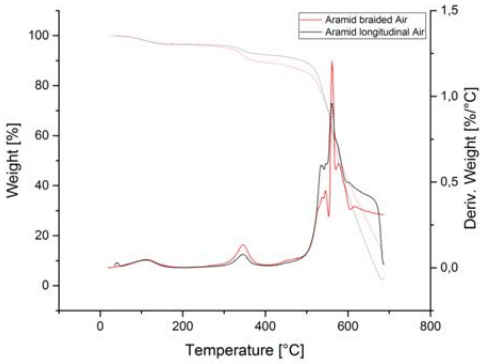

Figure 3.46: TGA/DTG Aramid air

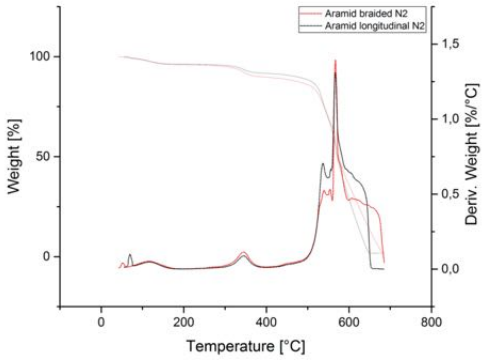

Figure 3.47: TGA/DTG Aramid N2

Table 3.4: TGA Aramid

		braided		longitudinal		Reference values [24]
		Air	N_2	Air	N_2	Air
$T_{firstdeg}$	[°C]	316	312	318	308	330
$T_{strongdeg}$	[°C]	521	522	522	524	530
$T_{4\%}$	[°C]	346	348	389	367	515

Degradation starts earlier within the braided textile. Table 3.4 displays that $T_{4\%}$ is under air 40°C higher in the longitudinal sample than in the braided one whereas $T_{firstdeg}$ and $T_{strongdeg}$ are almost the same in both samples.
One explanation for the earlier degradation of the outer and therefore the braided yarn is the pre-damage by UV- radiation. The inner yarn had another colour than the outer one what might be caused by radiation and damaged the braided yarn more than the inner, longitudinal one.
The overlay of TGA and DTG in figure 3.46 and 3.47 shows that the two steps occur at the same temperature. Also, the point of maximum degradation is located at the same temperature.

3.4 Tensile Test

The tensile test for the liner was carried out in two versions. With the specimen geometry following figure 2.8 and according to EN ISO 527-2. With the first version, only pipe 3 and pipe 4 were tested. Pipes 1 and 2 were tested without the narrowing in the middle of the specimen. But the clamps could not hold them, they got pulled out of them before the break.

The statistics of the two tensile tests in table 3.5 show that Young's modulus is more than half of the value [9] provides for a PA6 conditioned at 23°C/50%. This strengthens the assumption that the supposed filler is a softener.

The yield strength ϵ_y is nearly the same as [9] gives (40 N/mm^2). The strain at break ϵ_b is with 190% and 160% a little bit lower than in literature.

The tests carried out under norm conditions are providing almost the same material values as it is illustrated in table 3.6, but the norm conditions make them more reliable. The specimen was stored under other conditions so the moisture was detected after the tensile tests by storing the samples at 80°C and 0% humidity for 48 hours. The water content of the standard specification specimen is given in table 3.7.

Increasing moisture leads to a decrease in Young's modulus and strength at yield.

Table 3.5: Statistics tensile test pipe 3 no norm conditions

Series	E_t	σ_y	ϵ_y	σ_b	ϵ_b	b	h
n=4	N/mm^2	N/mm^2	%	N/mm^2	%	mm	mm
x	639	39,1	28,1	51,5	190,3	1,1	6,5
s	22,7	2,2	6,9	4,5	44,4	0,04	0,1
ν[%]	3,6	5,7	24,7	8,8	23,3	3,4	1,3

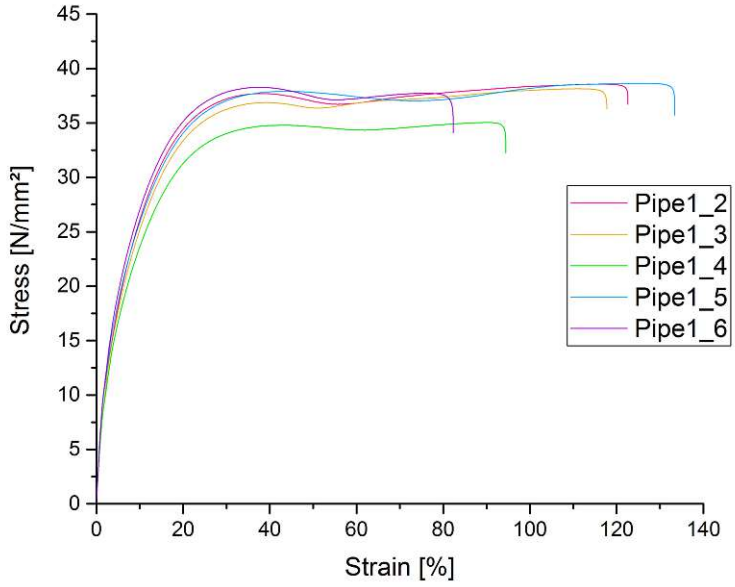

Figure 3.48: Stress - strain diagram pipe 1 according to EN ISO 527-1

Table 3.6: Statistics tensile test pipe 1 according to EN ISO 527-1

Series	E_t	σ_m	ϵ_m	σ_b	ϵ_b	b	h
n=8	N/mm^2	N/mm^2	%	N/mm^2	%	mm	mm
x	681	37,4	91	34,3	100	10,1	6,6
s	36,1	1,35	34	1,9	22	0,3	0
ν[%]	5,4	3,6	37	5,5	20,8	2,6	0

Table 3.7: Watercontent

	Pipe 1	Pipe 2	Pipe 3	Pipe 4
Watercontent [%]	0,98	0,98	0,98	0,98

3.4.1 Tensile Test Aramid

In table 3.8 the results of the tensile test of the Aramid fibres can be seen. Only the breaking strength was measured for the evaluation of the fibres.
The breaking strength is about 140N lower than specified in datasheet [3], where a breaking strength of 360N is published. The standard deviation is with 107N (48%) also quite high. However, 2 factors reduce the informative value of the measurements. That is, on the one hand, the non- standard measurement and on the other hand, the twist level of the fibres.
A standard measurement according to DIN EN 12562 was not possible because neither fibres in a length which is needed for the standard test, nor the clamp type for a standard test were available. So the yarn was wound around two cylinders, which caused that the yarn was not fixed as well as it would have been with clamps according to DIN EN 12562, but was a bit yielding. This is why the gradient at the beginning of the single curves and therefore Young's modulus in figure 3.49 is so small and it does not give a representative picture. That is the reason why only the maximum force was evaluated.
The missing information about the twist level of the yarn also makes it hard to make an authentic statement about the condition of the Aramid. When interwoven, the yarn has a twist level of 90tpm but it can not be said for sure, whether it stayed at 90tpm after separating the single yarn pieces from the fabric and clamping it into the testing machine. As it can be seen in 1.16, the twist level has a significant influence on the breaking strength.

Table 3.8: Statistics tensile test Aramid

Series	Breaking strength
n=9	N
x	225
s	107
ν[%]	48

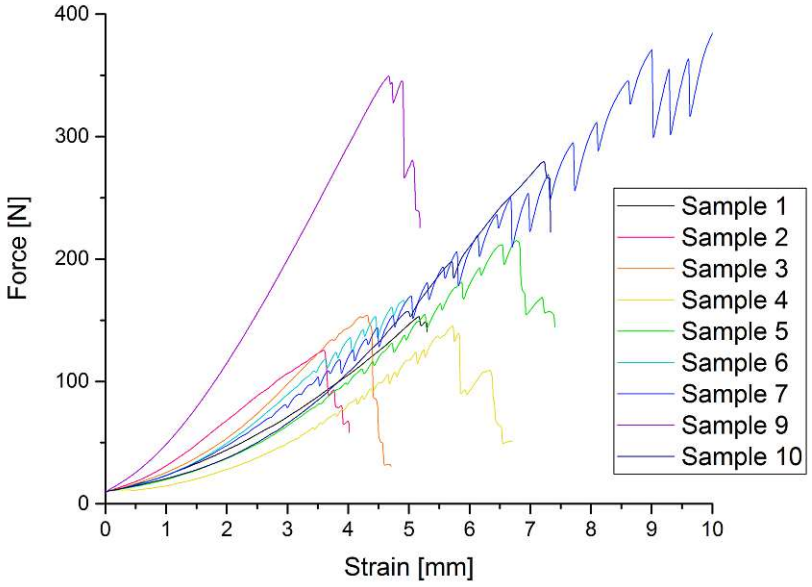

Figure 3.49: Force - strain curves Aramid

3.5 Charpy Notched Impact Test

The results for the Charpy notched impact tests are given in table 3.9 and 3.10. Sample 1.3 of pipe 1 was pre-damaged and is therefore not included in the statistics. The impact strength for PA6 is a_{CN}=25 kJ/m^2 – no break for a sample stored under 23°C and 50% humidity. The results received from the test are consistent. The impact strength is increasing with increasing moisture. If the filler is a softener, it also would also increase the impact strength.

Table 3.9: Charpy Notched Impact Test statistics Pipe 1

Sample	Energy	b	h	a_{CN}	Note
n=4	J	mm	mm	kJ/m^2	
1.1	7,90	10,02	6,6	120	hinge break
1.2	4,24	10,02	6,6	64	
1.3	2,21	9,91	6,6	34	pre- damaged
1.4	4,04	10,07	6,6	61	
1.5	4,01	10,15	6,6	60	
$\bar{x}$	5,05	10,07	6,6	76	
s	1,65	0,05	0	25,12	

Table 3.10: Charpy Notched Impact Test statistics Pipe 3

Sample	Energy	b	h	a_{CN}	Note
n=5	J	mm	mm	kJ/m^2	
3.1	4,14	10,02	6,6	63	
3.2	3,43	10,05	6,6	52	
3.3	8,18	10,15	6,6	122	hinge break
3.4	4,20	10,12	6,6	63	
3.5	5,87	10,01	6,6	89	
$\bar{x}$	5,15	10,07	6,6	78	
s	1,71	0,06	0	25,38	

3.6 EDX

The EDX spectra 3.50 of the liner material showed the following components:

- Carbon (C)
- Oxygen (O)

Besides H and N, these are the components from which Pa is made. A second recorded spectrum of the same sample at another point showed the same composition. Apart from gold, with which the sample was coated, no inorganic substances could be detected. This means that the additive, which was assumed to be a softener, must be organic. It could be a monomeric softener like polyvinyl alcohol (PVAL), linear polyurethane (TPU) or any other additive. If it were not an organic additive, another element should have been found, especially because the additive makes about 8% wt. in PA6. The EDX analysis does not allow any further interpretation at this point.

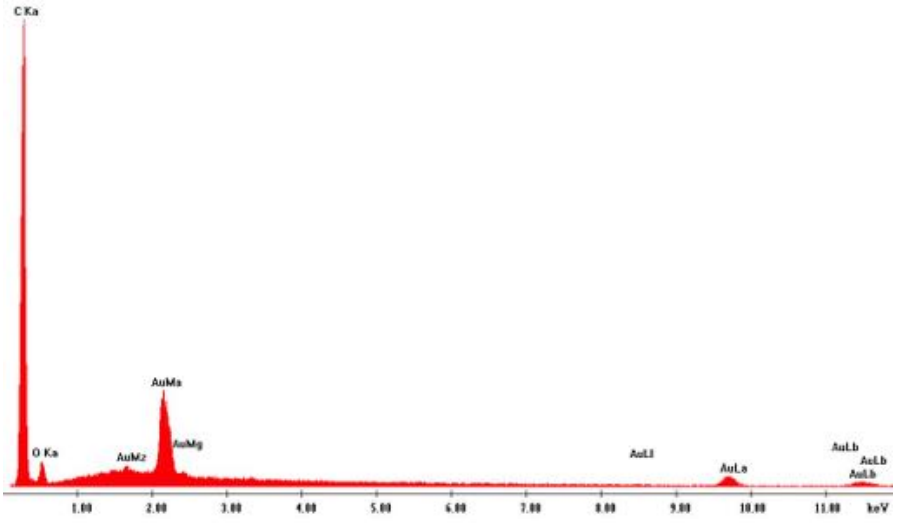

Figure 3.50: EDX spectra

4 Conclusion

The aim of the thesis was to test the ageing process of four segments of reinforced thermoplastic pipes (RTP). First of all, the materials, which the individual layers of the pipes are made of, had to be analysed and identified, since no data sheets have existed. After a preliminary characterization by means of DSC and FTIR, thermal, mechanical and optical analyses were carried out to determine if the pipes are aged. The investigations showed that the liner and the jacket are made of polyamide 6 (PA6) and the reinforcement of aramid (PPTA).
Since no reference samples were available, an obviously aged area of the liner at the end of the pipes was chosen for further analysis. That area was not protected by reinforcement and jacket and obvious ageing in form of cracks and discoloration was noticed (R_A, R_E). Specimen from this area were compared to those taken from areas covered by reinforcement and jacket.
For thermal analysis five samples were taken from each of the four pipes, distributed over the wall thickness. The sample preparation was performed with a microtome. The melting temperature T_m, crystallization temperature T_c and crystallinity X_c were in the expected range according to literature. The same behaviour could be found for all samples from the four tubes examined. T_m and T_c showed a slightly increased value on the inside and outside of the liner, which led to the assumption that X_c has also increased at the outer regions. This could not be proven in the course of the analysis. X_c is evenly distributed over the cross-section. Double melting peaks were also found in the layer and outer areas of the pipes, which are more prominent in the obviously ages samples (R_A, R_E) than in the presumably unaged samples (A, E). However, the double peaks could not be clearly assigned to ageing. In addition, a third peak at about 190°C occurs in the aged samples. This peak can be assigned to defect γ - crystals which melt and recrystallize to α - crystals. In the middle layers (B, C, D) no difference between

aged and non-aged samples was found.
For the FTIR investigations, the wall thickness was divided into 14 samples, which were also preparated with the microtome, to ensure a better resolution over the cross-section. It was assumed that, due to the multiple melting peaks in the DSC melting curves on the inside and outside of the pipes, a larger amount of γ - phase is present. At higher cooling rates as it can be found in the outer regions of moulded parts, the γ - phase is developing more strongly than in the inner regions with a smaller cooling rate. However, this could not be determined. Also, no different morphologies of PA6 could be attributed to the different colours across the cross-section of the liner. An XRD analysis would provide more precise information to this point. However by comparing the samples with those from the edge area, more informative observations could be made and conclusions about ageing could be drawn by examining the carbonyl band, NH-, and CH_2- stretching. Hereby clear ageing could be detected in the obviously aged samples compared to those samples from the hidden areas. However, care must be taken by this interpretation because no reference samples are available.
The TGA analysis, in connection with the mechanical investigations, brought revealing results. It could be determined that an additive is no longer present in the supposed areas, i.e. those not covered with reinforcement and jacket, but is still present in the covered areas of the liner. In this area, the additive is distributed more or less evenly over the cross-section. In the inner layers (B, C, D), the same amount of this additive could be found in both pipe sections, in the concealed and the exposed one. It must, therefore, have degraded or evaporated during the storage period. The initial assumption that it would be a plasticizer was confirmed by the mechanical analysis. Compared to the value in the literature, the liner material shows a significantly reduced Young‘s modulus and the yield stress figured well within an expected range. The Charpy impact strength delivers a much higher value than the literature suggests. These two facts strongly indicate that a plasticizer was used.
The examination of the jacket by means of the dye penetrant test showed that the cracks, found on the surface of the jacket, propagate up to about one-third of the wall thickness. No significant differences in the DSC-curves and values between jacket and liner were found, however, the jacket shows cracks which are located

on all four specimen. Nevertheless, since the jacket only serves to protect against mechanical stress and does not take any pressure, its condition can be classified as usable.

Since the tensile test of the aramid yarn was not performed according to the standard, the informative value must be seen as reduced. Although the average value of the maximum force is clearly below the value specified in the datasheets, a very high standard deviation has been obtained and some fibres still reach the specified value. In this case, a test according to the standard should be carried out to obtain a meaningful result.

In summary, after the optical, thermal and mechanical evaluation of all four pipes, it can be said that the individual tubes behave in the same way and show similar material values. The absence of suitable reference material only allows a comparison with an obviously aged sample and only testing for relative ageing can be executed. All in all, the pipes show good properties in the areas away from the edge and no massive ageing can be assumed. In order to obtain a more substantiated statement, some samples should be kept under artificial ageing and examined after that. Furthermore, a test on the tube- test- bench would be a promising method to check the suitability of pipes for their use regarding maximum temperature and maximum pressure.

Bibliography

[1] Teijin Aramid BV. *Research note*. unpublished, 2012.

[2] DIN 60 900 Teil 2. *Garne, Beschreibung im Tex-System*. Juli 1988.

[3] Teijin Aramid BV. *Mechanical properties of Twaron yarn type 1008*. unpublished, 2012.

[4] D. Braun. *Kleine Geschichte der Kunststoffe*. München: Hanser, 2013.

[5] M. Gilbert. *Brydson's plastics materials*. Amsterdam: Elsevier, 2017.

[6] P. Eyerer; T. Hirth; P. Elsner. *Polymer Engineering*. Berlin, Heidelberg: Springer-Verlag, 2008.

[7] E. Baur; T. A. Osswald; N. Rudolph. *Plastics handbook : the resource for plastics engineers*. München, Cincinnati: Hanser, 2019.

[8] Schwarz/Ebeling (Hrsg.) *Kunststoffkunde : Aufbau, Eigenschaften, Verarbeitung, Anwendungen der Thermoplaste, Duroplaste und Elastomere*. Würzburg: Vogel, 2005.

[9] H. Domininghaus. *Die Kunststoffe und ihre Eigenschaften*. Düsseldorf: VDI-Verl., 2008.

[10] W. Grellmann; S. Seidler. *Polymer Testing*. München: Hanser, 2007.

[11] G. W. H. Höhne; W. F. Hemminger; H. J. Flammersheim. *Differential scanning calorimetry : with 19 tables*. Berlin [u.a.]: Springer, 2003.

[12] E. Parodi; G. W. M. Peters; L. E. Govaert. "Prediction of plasticity-controlled failure in polyamide 6: Influence of temperature and relative humidity". In: *Journal of Applied Polymer Science, Vol. 135* (2018), p. 45942.

[13] A. Frick; C. Stern. *Praktische Kunststoffprüfung*. München: Hanser, 2011.

[14] N. Scoutaris; K. Vithani; I. Slipper; B. Chowdhry; D. Douroumis. "SEM/EDX and confocal Raman microscopy as complementary tools for the characterization of pharmaceutical tablets". In: *International Journal of Pharmaceutics, Vol. 470* (2014), pp. 88–98.

[15] K. Shi; L. Ye; G. Li. "Thermal oxidative aging behavior and stabilizing mechanism of highly oriented polyamide 6". In: *J Therm Anal Calorim, Vol. 126* (2016), pp. 795–805.

[16] Y. Shu; L. Ye; T. Yang. "Study on the Long-Term Thermal-Oxidative Aging Behavior of Polyamide 6". In: *Journal of Applied Polymer Science, Vol. 110* (2008), pp. 945–957.

[17] S. Z. Kunchimon; M. Tausif; P. Goswami; V. Cheung. "Polyamide 6 and thermoplastic polyurethane recycled hybrid Fibres via twin-screw melt extrusion". In: *Journal of Polymer Research, Vol. 6* (2019), p. 162.

[18] I. Kolesov; R. Androsch. "The rigid amorphous fraction of cold-crystallized polyamide 6". In: *Polymer 53* (2012), pp. 4770–4777.

[19] S. Aitha; N. Vasanthan. "Effect of cellulose nanocrystals on crystallization, morphology and phase transition of polyamide 6". In: *Composite Interfaces, 27:4* (2019), pp. 371–384.

[20] W. Donga; P. Gijsman. "Influence of temperature on the thermo-oxidative degradation of polyamide 6 films". In: *Polymer Degradation and Stability, Vol. 95* (2010), pp. 1054–1062.

[21] L. Sang; C. Wang; Y. Wang; Z. Wei. "Thermo-oxidative ageing effect on mechanical properties and morphology of short fibre reinforced polyamide composites – comparison of carbon and glass fibres". In: *The Royal Society of Chemistry, Vol. 7* (2017), pp. 43334–43344.

[22] M. Herrera; G. Matuschek; A. Kettrup. "Main products and kinetics of the thermal degradation of polyamides". In: *Chemosphere, Vol. 42* (2001), pp. 601–607.

[23] S. Mouffok; M. Kaci. "Artificial weathering effect on the structure and properties of polypropylene/polyamide-6 blends compatibilized with PP-g-MA". In: *Journal of Applied Polymer Science, Vol. 132* (2015), p. 41722.

[24] K. E. Perepelkin; I. V. Andreeva; E. A. Pakshver; I. Yu. Morgoeva. "Thermal characteristics of para-aramid fibres". In: *Fibre Chemistry, Vol. 35, No. 4* (2003), pp. 265–269.

[25] C. Connor; M. M. Chadwick. "Characterization of absorbed water in aramid fibre by nuclear magnetic resonance". In: *Journal of Materials Science, Vol. 31* (1996), pp. 3871–3877.

List of Figures

1.1 Pipe 1 . . . 2
1.2 Pipe 2 . . . 2
1.3 Pipe 3 . . . 2
1.4 Pipe 4 . . . 2
1.5 Imprint on pipe 3 . . . 3
1.6 Cross section . . . 3
1.7 End of pipe 1 . . . 4
1.8 End of pipe 2 . . . 4
1.9 End of pipe 3 . . . 4
1.10 End of pipe 4 . . . 4
1.11 Reinforcement outside . . . 5
1.12 Reinforcement inside . . . 5
1.13 Reinforcement braided . . . 5
1.14 Reinforcement longitudinal . . . 5
1.15 Properties of various Twaron type 1008 yarn [3] . . . 6
1.16 Breaking strength of Twaron type 1008 at various twist levels [3] . . . 6
1.17 Jacket pipe 1 . . . 7
1.18 Jacket pipe 2 . . . 7
1.19 Jacket pipe 3 . . . 7
1.20 Jacket pipe 4 . . . 7
1.21 Inside of the jacket . . . 8
1.22 -CONH- group [6] . . . 9
1.23 Aliphatic molecule [6] . . . 10
1.24 Aromatic molecule [6] . . . 10
1.25 PA6 with -CONH- group [6] . . . 11
1.26 PPTA [6] . . . 11

1.27 Molecular structure of PA6 and PA66 [9] 13

2.1 DSC measuring cell [10] 15
2.2 Division of the cross section 17
2.3 Various stress-strain curves [10] 19
2.4 Influence of moisture on PA [12] 20
2.5 Conditioning of PA [9] 20
2.6 Charpy notched impact test arrangement [10] edited 22
2.7 Pre-cut of tensile test specimen 22
2.8 Tensile test specimen 23
2.9 Notched Charpy impact test specimen 23
2.10 ISO 527-1 1B specimen 24
2.11 ISO 527-1 1B specimen 24
2.12 FTIR operating mode [10] edited 25
2.13 Gold-coated cryobreak 27

3.1 Jacket 28
3.2 Aged end of pipe 1 29
3.3 Uncovered liner of pipe 1 29
3.4 Color penetration testing 30
3.5 Depth of cracks 30
3.6 Cross section 30
3.7 Melting temperatures 31
3.8 Melting peaks of pipe 2 with offset 32
3.9 Crystallinity 33
3.10 Crystallization peaks of pipe 2 33
3.11 Crystallisazion temperature 34
3.12 Melting peaks from aged area of pipe 1 35
3.13 Melting temperatures 35
3.14 Melting peaks of Jacket from pipe 1 36
3.15 FTIR spectra pipe 1 37
3.16 FTIR spectra PA6 [20] 37
3.17 Carbonyl group 38
3.18 CH_2 - Streching 39

3.19 NH - Streching . . . 39
3.20 Carbonyl group pipe1 and pipe 1R . . . 40
3.21 CH_2 - Stretching pipe 1 and pipe 1R . . . 41
3.22 CH_2 - Stretching pipe 1 and pipe 1R . . . 41
3.23 NH - Stretching pipe 1 and pipe 1R . . . 42
3.24 FTIR spectra . . . 43
3.25 Amorphous phase . . . 44
3.26 Intensity at 1124 cm^{-1} . . . 44
3.27 Hexagonal phase . . . 45
3.28 Intensity at 975 cm^{-1} . . . 45
3.29 Monoclinic phase . . . 45
3.30 Intensity at 930 cm^{-1} . . . 45
3.31 TGA curve pipe 1 air . . . 46
3.32 Waterstep pipe 3 air . . . 46
3.33 3% step . . . 47
3.34 T_{300} pipe4 air . . . 48
3.35 T_{300} pipe 4 N_2 . . . 48
3.36 T_{300} pipe 1 R air . . . 48
3.37 T_{300} pipe 1 R N_2 . . . 48
3.38 TGA/DTG A . . . 49
3.39 TGA/DTG E . . . 49
3.40 $T_{3\%\ step}$ air . . . 50
3.41 $T_{3\%\ step}$ N_2 . . . 50
3.42 T_{maxdeg} air . . . 50
3.43 m_{maxdeg} air . . . 50
3.44 TGA Aramid under N_2 . . . 52
3.45 TGA Aramid under Air . . . 52
3.46 TGA/DTG Aramid air . . . 52
3.47 TGA/DTG Aramid N2 . . . 52
3.48 Stress - strain diagram pipe 1 according to EN ISO 527-1 . . . 55
3.49 Force - strain curves Aramid . . . 57
3.50 EDX spectra . . . 59

List of Tables

2.1 Physical and chemical causes for DSC peaks [10] 15
2.2 Temperature program 16
2.3 Resolution of the FTIR analysis 26

3.1 Characteristic peaks 37
3.2 m_{300} pipe 4 unaged 48
3.3 m_{300} pipe 1 aged 48
3.4 TGA Aramid 52
3.5 Statistics tensile test pipe 3 no norm conditions 54
3.6 Statistics tensile test pipe 1 according to EN ISO 527-1 55
3.7 Watercontent 55
3.8 Statistics tensile test Aramid 56
3.9 Charpy Notched Impact Test statistics Pipe 1 58
3.10 Charpy Notched Impact Test statistics Pipe 3 58

Appendix

Dye Penetrant Test

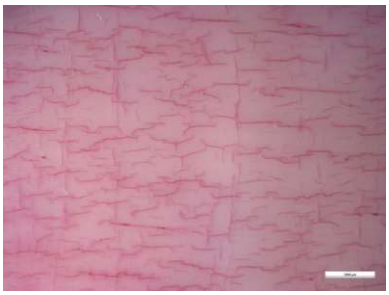

Color penetration testing pipe 1

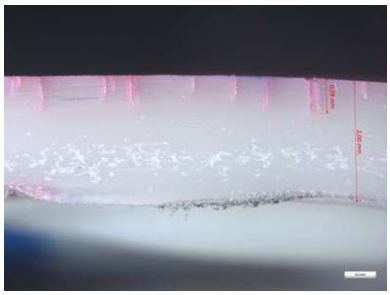

Color penetration testing grounded pipe 1

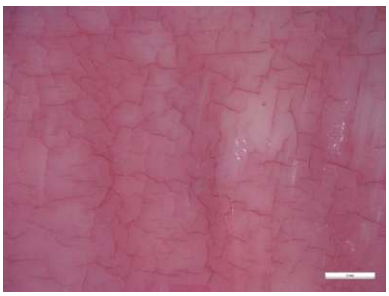

Color penetration testing pipe 2

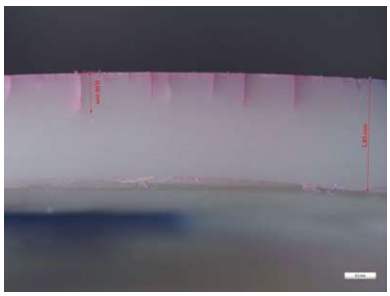

Color penetration testing grounded pipe 2

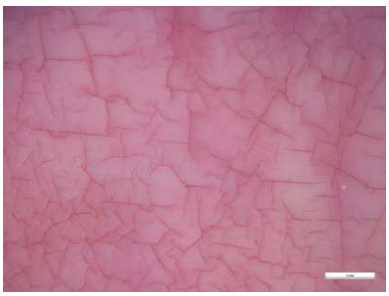

Color penetration testing pipe 3

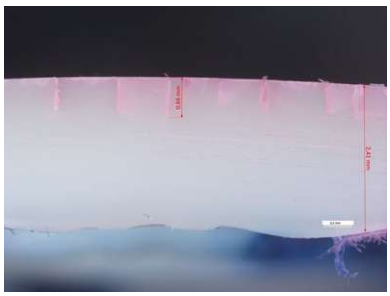

Color penetration testing grounded pipe 3

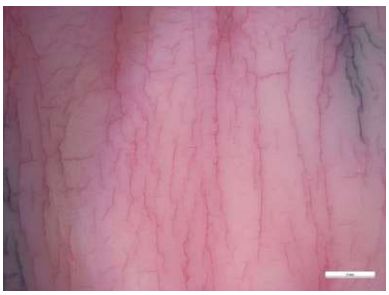

Color penetration testing pipe 4

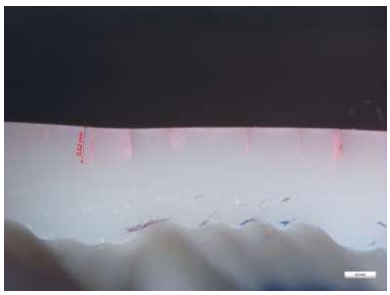

Color penetration testing grounded pipe 4

DSC

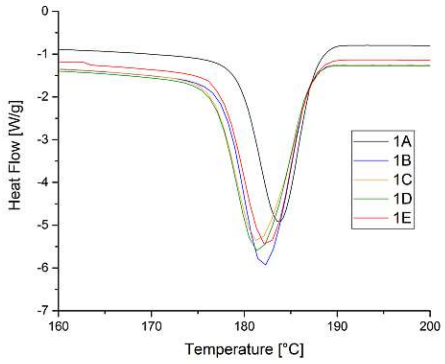

Crystallization peak pipe 1

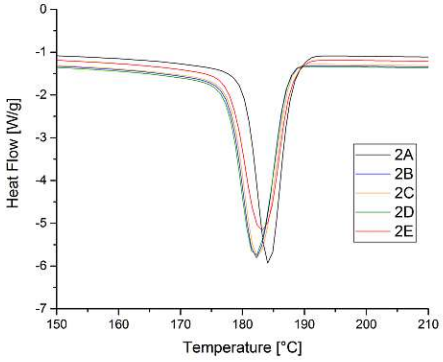

Crystallization peak pipe 2

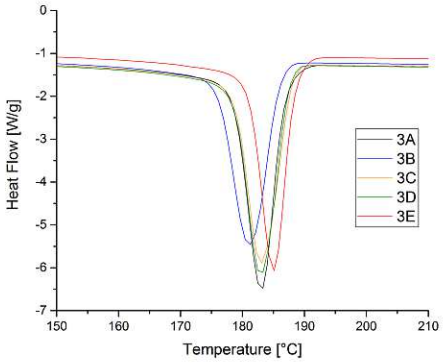

Crystallization peak pipe 3

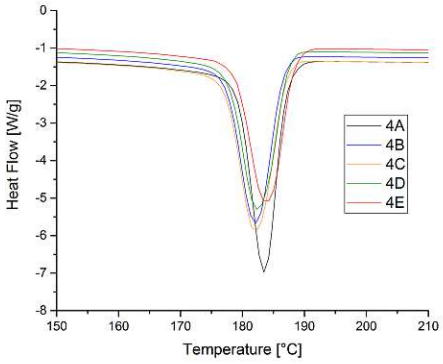

Crystallization peak pipe 4

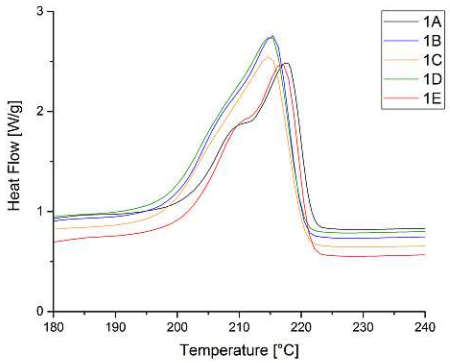

Melting peak pipe 1

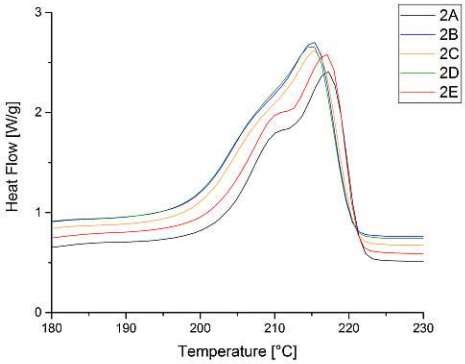

Melting peak pipe 2

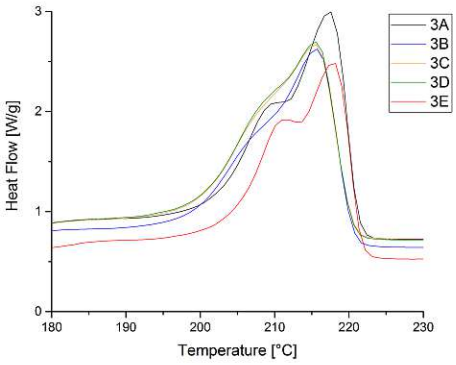

Melting peak pipe 3

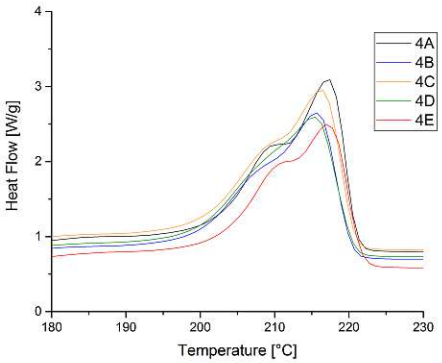

Melting peak pipe 4

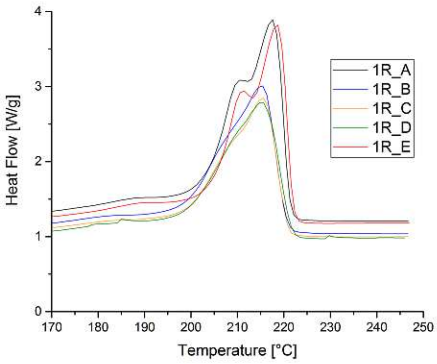

Melting peak pipe 1 R

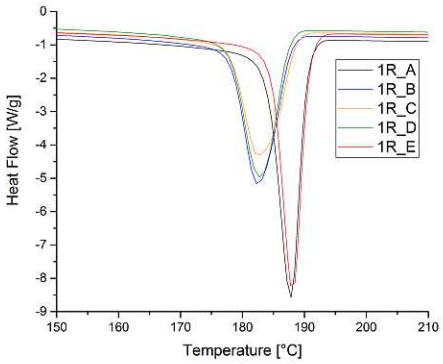

Crystallization peak pipe 1 R

TGA

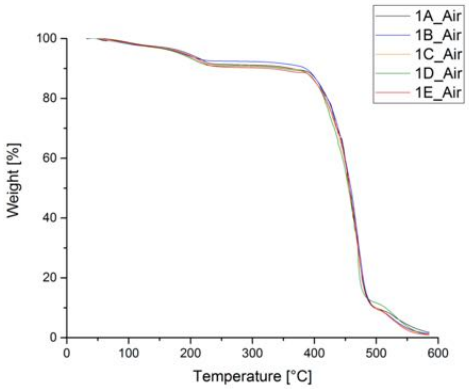

TGA Pipe 1 air

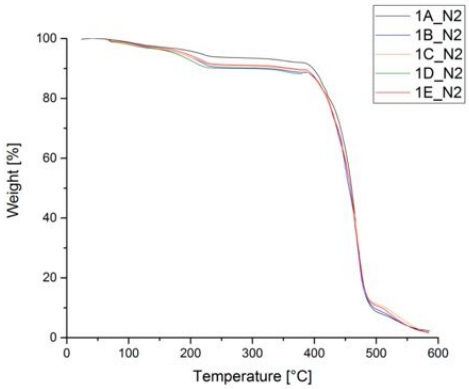

TGA Pipe 1 N_2

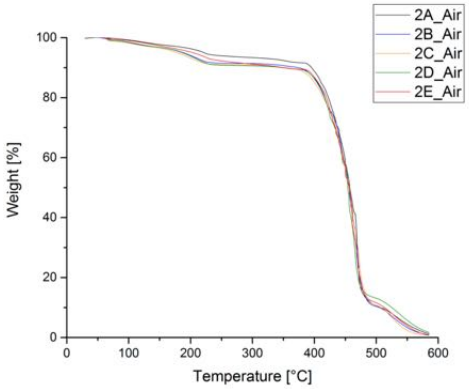

TGA Pipe 2 air

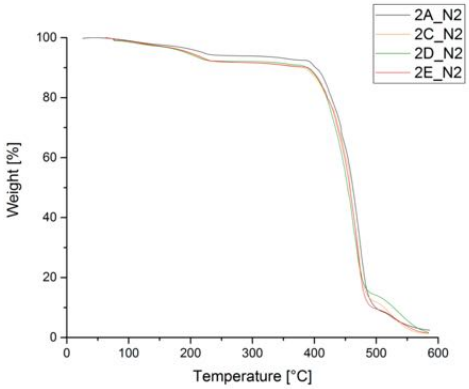

TGA Pipe 2 N_2

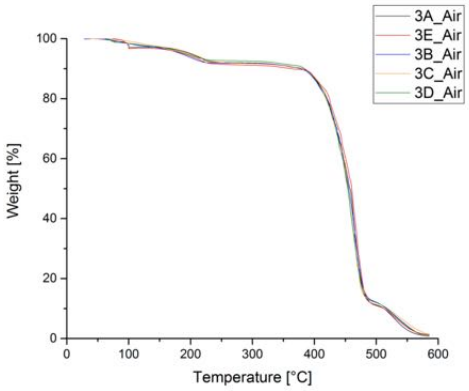

TGA Pipe 3 air

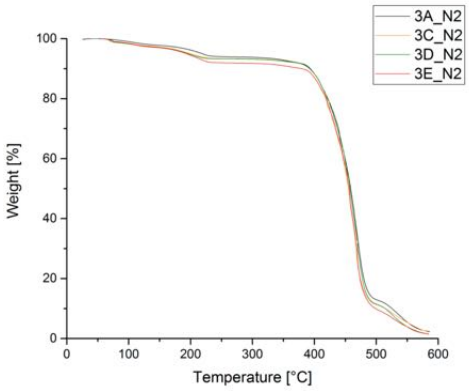

TGA Pipe 3 N_2

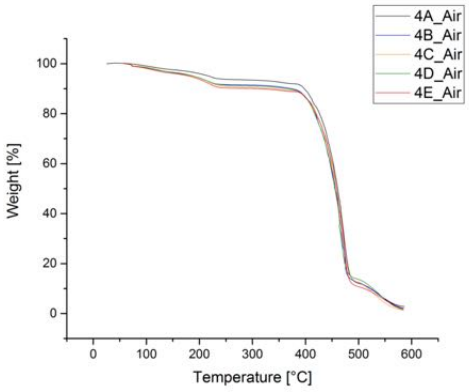

TGA Pipe 4 air

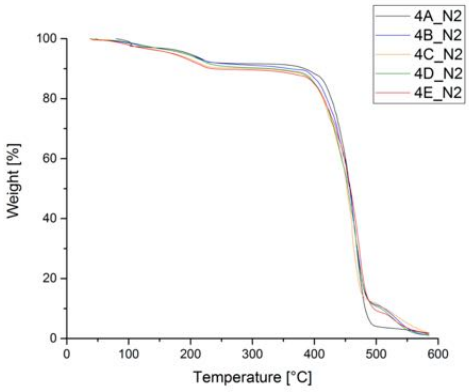

TGA Pipe 4 N_2

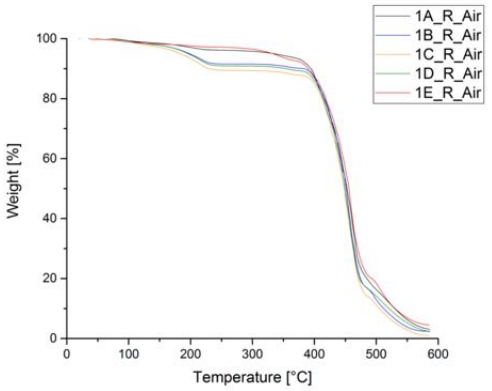

TGA 1 R air

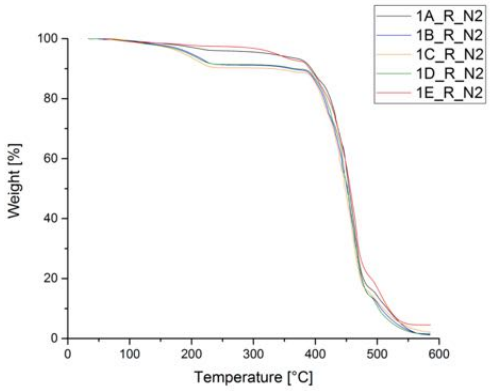

TGA 1 R N_2

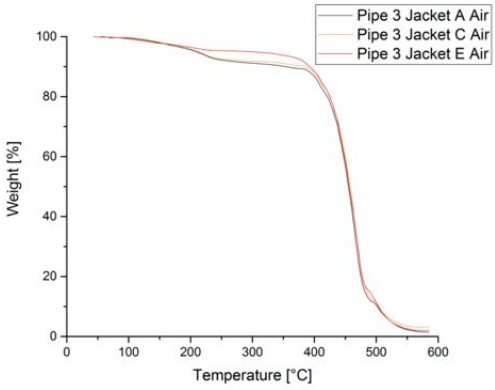

TGA Pipe 3 Jacket air

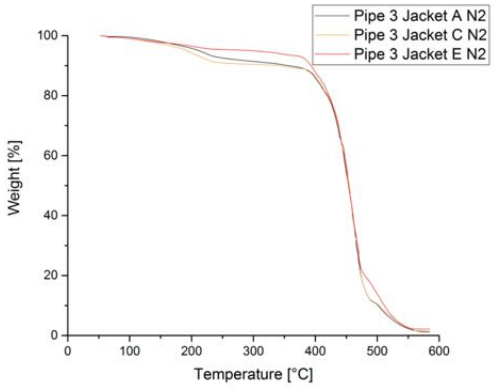

TGA Pipe 3 Jacket N_2

Tensile Test

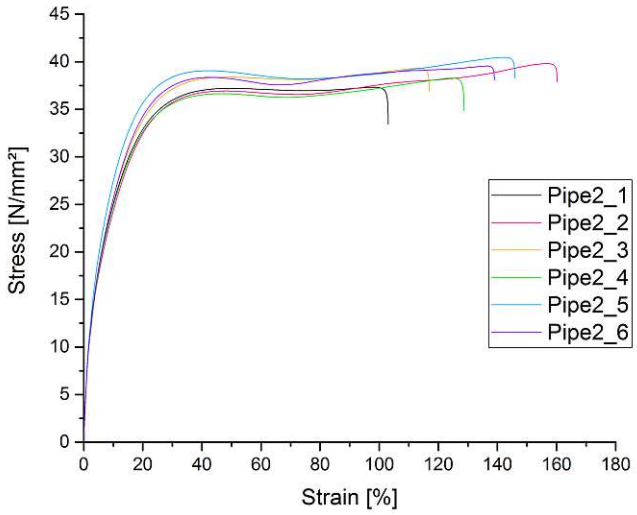

Stress - strain diagram pipe 2

Statistics tensile test pipe 2

Series	E_t	σ_m	ϵ_m	σ_b	ϵ_b	b	h
n=8	N/mm^2	N/mm^2	%	N/mm^2	%	mm	mm
x	692	39,1	130	36,6	130	10,3	6,6
s	17,2	1,13	21	2	21	0,5	0
ν[%]	2,5	2,9	16,5	5,4	15,6	4,7	0

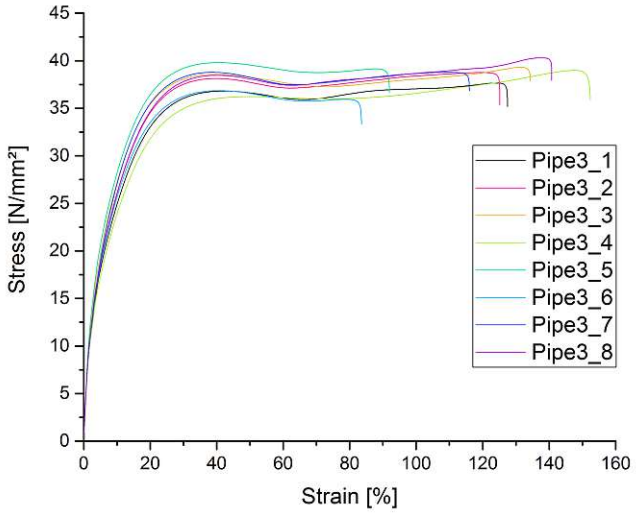

Stress - strain diagram pipe 3

Statistics tensile test pipe 3

Series	E_t	σ_m	ϵ_m	σ_b	ϵ_b	b	h
n=8	N/mm^2	N/mm^2	%	N/mm^2	%	mm	mm
x	713	38,8	110	36,1	120	10,2	6,6
s	20	1,1	42	1,5	24	0,7	0
ν[%]	2,8	2,9	39,2	4,3	19,4	6,6	0

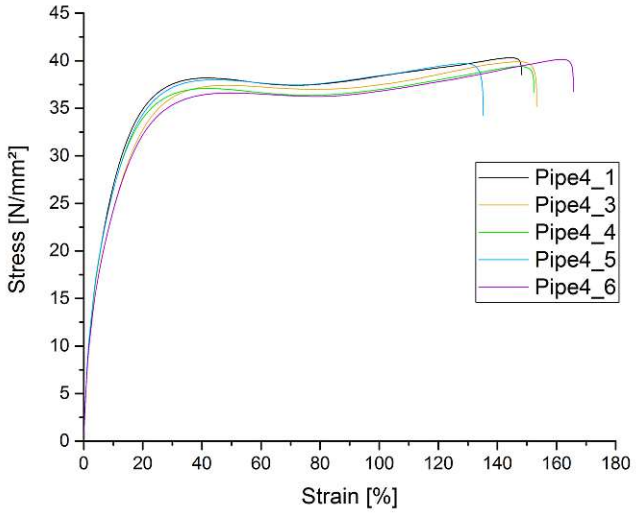

Stress - strain diagram pipe 4

Statistics tensile test pipe 4

Series	E_t	σ_m	ϵ_m	σ_b	ϵ_b	b	h
n=8	N/mm^2	N/mm^2	%	N/mm^2	%	mm	mm
x	696	39,9	150	36,3	150	10,1	6,6
s	12,4	0,4	12	1,6	11	0,5	0
ν[%]	1,8	0,9	8,2	4,5	7,3	4,8	0

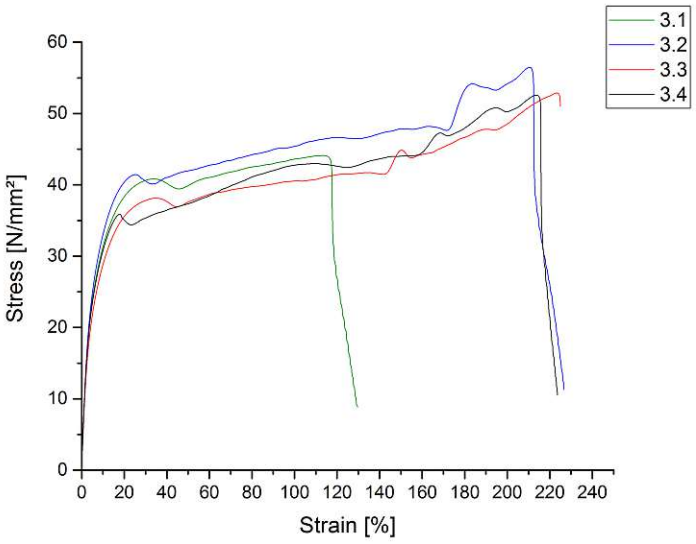

Stress - strain diagram pipe 3 non standard

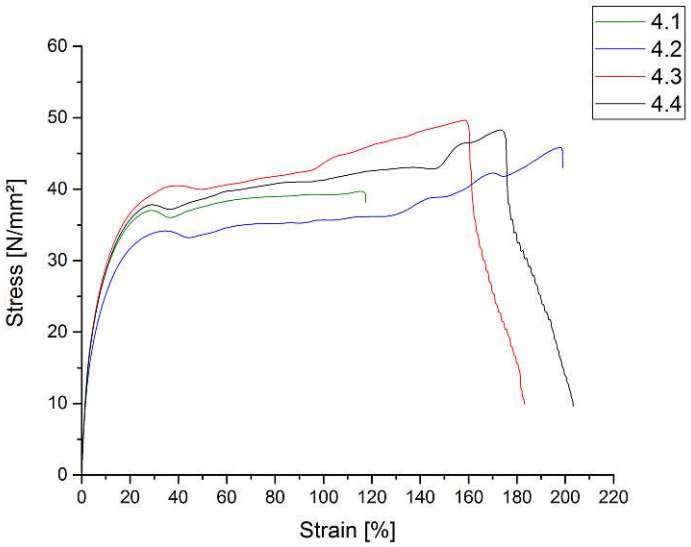

Stress - strain diagram pipe 4 non standard

Statistics tensile test pipe 4 non standard

Series	E_t	σ_y	ϵ_y	σ_b	ϵ_b	b	h
n=4	N/mm^2	N/mm^2	%	N/mm^2	%	mm	mm
x	607	37,4	33,1	45,9	161,1	1	6,7
s	40,4	2,3	4,2	3,8	30	0,1	0,1
ν[%]	6,7	6,1	12,6	8,3	18,6	5,9	0,7

FTIR

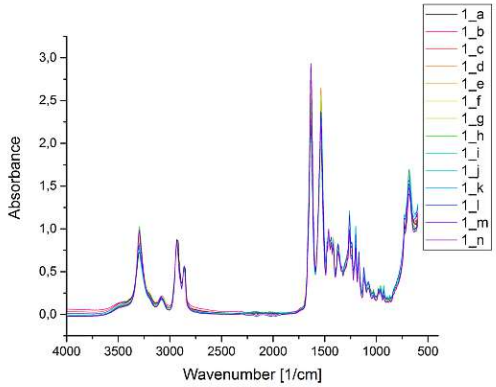

FTIR spectra pipe 1

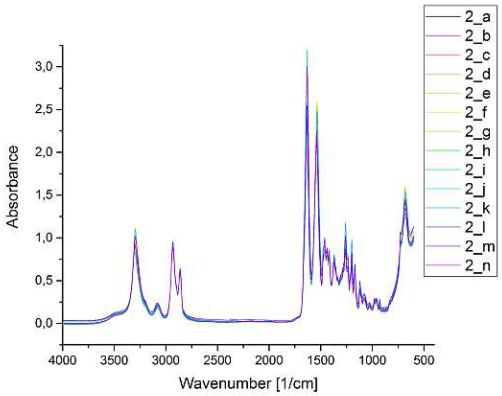

FTIR spectra pipe 2

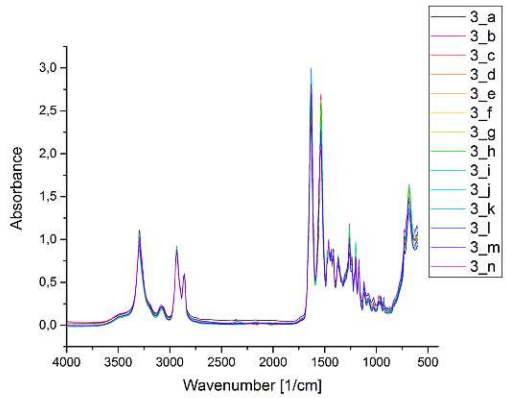

FTIR spectra pipe 3

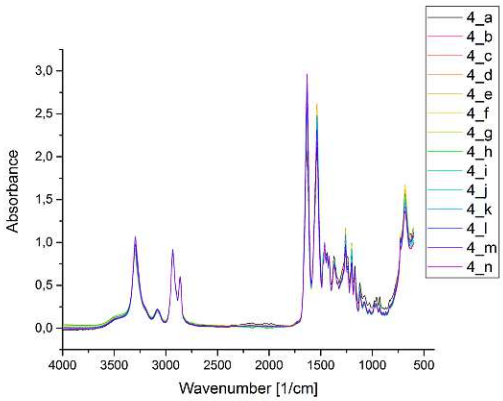

FTIR spectra pipe 4

MECHANICAL PROPERTIES OF TWARON YARN TYPE 1008

Introduction
Twaron yarn type 1008 is the standard type for oil and gas applications.

The standard delivery program for Twaron 1008 is:
1100 dtex Z120
1680 dtex Z90
2520 dtex Z75
3360 dtex Z60

Flat (untwisted) yarn can be used but is not recommended for some applications.
Other dtex's and twist levels are available on request.

This publication provides detailed data on the properties of Twaron 1008 yarn.
The mechanical properties of Twaron yarns are determined according to standard procedures as described in "Test methods for p-aramid yarn (SMA latest version)".

Properties of Twaron 1008 yarn

Twaron 1008 (dtex)		**1100 F1000**	**1680 F1000**	**2520 F1000**	**3360 F2000**
Linear density	dtex	1135	1735	2600	3500
Breaking strength	N	242	360	530	705
Elongation at break	%	3.35	3.45	3.8	3.6
Force at specified elongation 1%	N	62	88	117	170
Loop breaking strength	N	211	310	431	643
Chord modulus	GPa	80	72	67	72
Measured at twist level	tpm	120	90	75	60

Representative force-elongation diagram of Twaron 1008 yarn

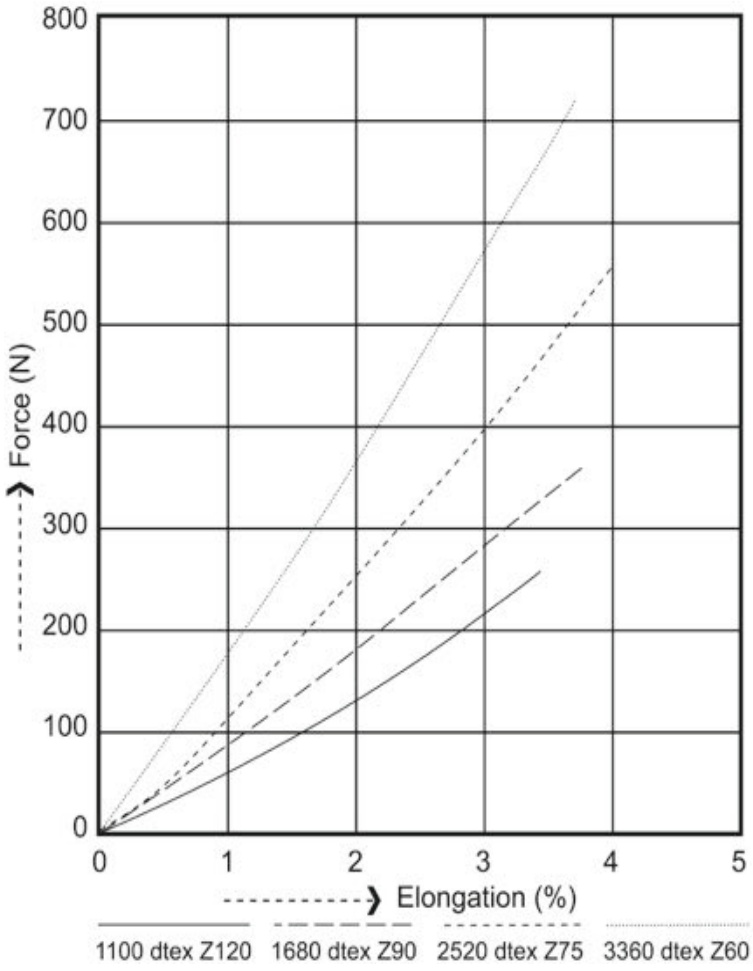

Influence of twist level on tensile strength

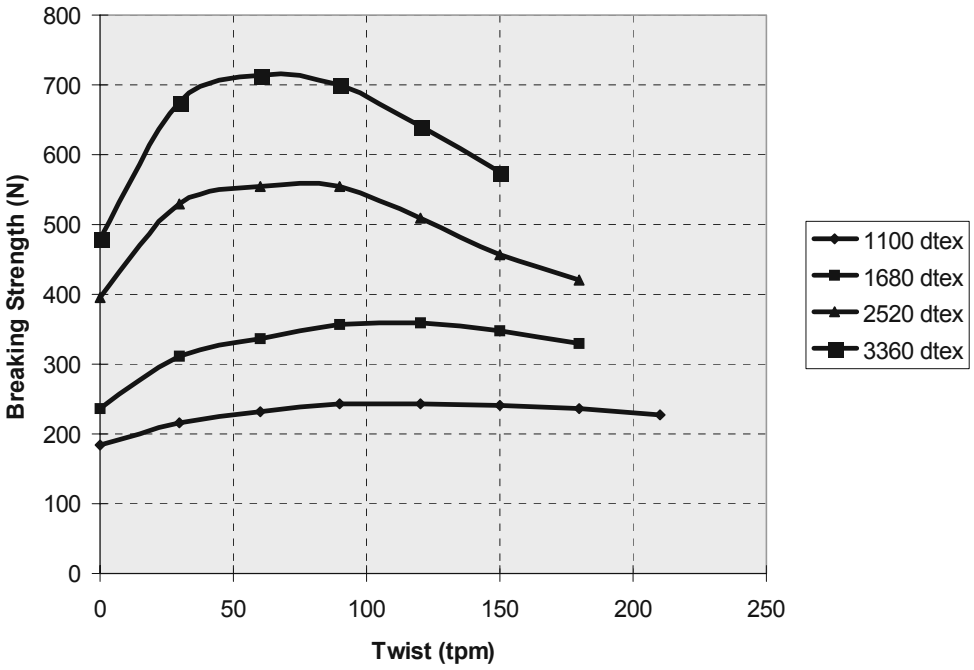

TEIJIN ARAMID BV
Westervoortsedijk 73
P. O. Box 9600
6800 TC Arnhem
The Netherlands
TEL. + 31 26 366 24 23
FAX. + 31 26 366 53 93
Email: information@teijinaramid.com
www.teijinaramid.com

For further information, please contact:

Oil & Gas Dept.
TEL. +31 26 366 55 33
FAX. +31 26 366 41 10
Email: oilandgas@teijinaramid.com

RESEARCH NOTE

TEIJIN

Technical Fiber Applications

To J. Aherne - QER
From E.E.W. Bottema
Date May 31, 2012
Subject **Properties Polyflow samples / Twaron 1008**
Copies To M. Tiwari - QRE

Summary
Polyflow Inc. uses Twaron as reinforcement yarn in a hose/pipe construction to transport onshore oil and/or gas. Polyflow Inc. sent a field tested pipe sample and asked us to determine the residual strength of the Twaron reinforcement in the pipe after ageing compared to a virgin hose.

The aged sample was taken from a live flow line which had been installed in Germany running at 40-50 bar of pressure flowing Natural gas, Brine, Oil and H_2S(80,000 ppm). It operated continuously for approximately 18 months after which time a section was removed for further examination.

Teijin Aramid tested the braid in the sample and compared it to a new sample of pipe to see if there was any degradation in the braid (Twaron) material.

Remark:
Only a short length of pipe was available. As a result the yarns specimens isolated from the pipe sample are short in length with the result that measuring according to the standard (ASTM) procedures was not possible. In this respect test settings used in this evaluation differs from the standard test procedure. Every effort was taken to ensure that the ASTM procedure was followed as much as possible irrespective of the short nature of the samples.

The obtained results give an indication if there is any degradation of the Twaron.

Material:
Photographs are shown in the Appendix B

Polyflow samples: (Appendix B)

1. Braided hose sample
2. Pipe sample after pressurized test for 18 months

Test procedure:

The tensile properties are determined according ASTM D7269 [1] and Teijin Aramid Standard Method of Analysis HS 3.01.29 [2]

Deviation from the standard test procedure, due to short sample lengths, are the used gauge length and test speed.
Also the clamp type used in this evaluation differs from the norm. Due to the small gauge length setting smaller clamps (Instron cat nr. 2714-004) are used for the determination of the tensile strength.
For the pipe samples a gauge length setting of 120 mm is used. (test speed 60 mm/min)

Results:
A table is shown in Appendix E.
Due to the lack of sample the results are indicative only.

Pipe sample:
The yarn specimens isolated from the field tested pipe sample do not show strength loss in the yarn in relation to the yarns taken from a virgin hose. The breaking strength obtained of the Twaron 1680x3 dtex is about 910 N. It seems to be that there is no degradation of the Twaron due to the service conditions (18months at roughly 40ºC and 40 to 50 bar continuous pressure with a mix of natural gas, brine, hydrocarbons and H_2S at 80,000ppm).

Our intention was to determine the viscosity of the Twaron yarn samples. This was to be a cross check to verify, using another method, that the material had not degraded. However due to a tacky coating on the 4 end tape the Twaron did not dissolve and hence the viscosity could therefore not be determined.

Summary and conclusions:

- The test indicates that no strength loss (degradation) is obtained in the yarn samples isolated from the field tested pipe sample
- Ideally we would like to have a larger section of pipe in order to conform to all requirements of the ASTM tensile test method and to provide a statistical analysis of the degradation ,or lack of, of the Twaron reinforcement and to ultimately provide a design-life curve for the material.

References:

[1] ASTM 7269 Standard Test Methods for Tensile Testing of Aramid Yarns
[2] SMA HS 3.01.29 Determination of the force elongation properties of P-aramid filament yarns

Appendix B: Polyflow samples

1: Braided hose sample

2: Field tested pipe sample after 18 months

Note: The pipe collapsed at the end of the test. The internal fluid was removed from the pipe section to be examined however it was still under external hydrostatic pressure. As a result the liner collapsed. In spite of this the braid residual strength seems to not be effected.

TEIJIN

Appendix E: Results Polyflow hose and pipe sample

				Material	Braided hose 1500/3				Pipe sample			
				Remark	Braided		Long		Braided		Long	
				Marker colour								
	Opdracht Y5787				Party 10				Party 11			
	Spoeltype 1			Number of spools	1		1		1			
Test	Description	1st	2nd	Unit	x	± c.i.	x	± c.i.	x	± c.i.		Samples to short for testing
number of singles tested (1500/3 level)					5		5		15			
	Black spots on yarn											
BS	**Breaking strength**			**N**	**900**	**± 80**	**880**	**± 150**	**910**	**± 90**		**NA**
BS-RS	Retained strength			%	95.8 {2}		95.7 {3}		101.1 {4}			
EAB	Elongation at break			%	3.8	± 0.26	3.95	± 0.34	3.78	± 0.35		
EAR	Elong.at rupture			%	3.8	± 0.26	3.95	± 0.34	3.78	± 0.35		
FASE	Force at spec.elong.	0.3		N	47	± 6	43	± 6	39.9	± 4.2		
FASE	Force at spec.elong.	0.5		N	87	± 12	80	± 11	76	± 8		
FASE	Force at spec.elong.	1		N	201	± 21	185	± 19	188	± 14		
FASE	Force at spec.elong.	2		N	448	± 37	411	± 30	442	± 25		
FASE	Force at spec.elong.	3		N	705	± 52	652	± 47	712	± 34		
CM	Chord modulus			mN/tex	46300	± 3100	43000	± 2300	47200	± 2100		

{2} BS-RS in relation to Braider Not run
{3} BS-RS in relation to std Long Not run
{4} BS-RS in relation to Braided hose